ALMA MATER STUDIORUM – UNIVERSITÀ DI BOLOGNA

CAMPUS DI CESENA

DEPARTMENT OF ELECTRICAL, ELECTRONIC, AND INFORMATION ENGINEERING - "Guglielmo Marconi" – "DEI"

MASTER'S DEGREE IN BIOMEDICAL ENGINEERING:

CURRICULUM OF BIOENGINEERING OF HUMAN MOVEMENT

Dissertation on:

PREDICTING CLINICAL OUTCOME OF FRACTURE FIXATION – A BIOMECHANICAL STUDY BASED ON RETROSPECTIVE CLINICAL DATA

Thesis in:

MECHANICS OF BIOLOGICAL TISSUES

Supervisors:

Prof. Ing. Luca Cristofolini

Dr. Rer. Medic. Adam Trepczynski

Dr. Ing. Mark Heyland

Candidate:

Matteo Gabriele

Session VI

Academic Year 2022/23

INDEX OF CONTENTS

1. STATE OF THE ART OF BONE FRACTURE HEALING 6
1.1 Bone Biology 6
1.2 Bone fractures 8
1.3 Primary and secondary repair mechanisms 9
1.4 Stages of fracture repair 9
1.4.1 Inflammatory response 9
1.4.2 Soft callus (cartilage) formation 10
1.4.3 Hard callus formation (endochondral ossification) 11
1.4.4 Bone remodelling 11
2. TREATMENT AND ASSESSMENT OF BONE FRACTURES 13
2.1 Fracture classification (AO/OTA) 13
2.2 Fracture treatment strategies 16
2.2.1 Fracture fixation 16
2.2.2 Cell-based therapies 17
2.3 Assessment of fracture healing 18
2.4 Objective of the study 20
3. RADIOLOGIC IMAGE ANALYSIS OF FRACTURE HEALING 21
3.1 Materials and Methods 21
3.1.1 Subjects 21
3.1.2 Preliminary Analysis 23
3.2 Results 25
3.3 Limitations and Discussion 30
4. CALLUS SIZE AND DENSITY DEVELOPMENT AFTER LOWER-LIMB FRACTURE FIXATION 31
4.1 Materials and Methods 31
4.1.1 Subjects 31
4.1.2 X-ray assessment 31
4.1.3 In silico model 32
4.1.4 Statistical analysis 33
4.2 Results 34
4.2.1 Femur 34
4.2.2 Tibia 36
4.2.3 Comparison between femur and tibia 39
4.2.4 Fixation treatment 41
4.2.5 Finite Element Analysis (FEA) strain component correlations with callus density and size 45

4.3 Limitations and Discussion....46
5. ANALYSIS OF JOINT LOADING RELATIONSHIP WITH MULTIPLE PHYSIOLOGICAL FACTORS....47
5.1 Materials and Methods....47
5.1.1 CAMS-Knee database....47
5.1.2 Musculoskeletal modelling....47
5.1.3 Subjects....48
5.2 Results....50
5.3 Limitations and Discussion....53
6. CONCLUSIONS....54
REFERENCES....56
ACKNOWLEDGEMENTS....60

ABSTRACT

Bone fracture healing is a complex and multifaceted process. Several factors affect the development of new callus such as fixation type, configuration, fracture characteristics and patient's related factors. This study aims to deeper understand the influence of fracture fixation on bone healing processes. The thesis was subdivided into three main parts, assessing the objective from different perspectives. Firstly, validation of the mRUST scoring system was conducted, revealing its utility in evaluating fracture healing stages via Intraclass Correlation Coefficients between ratings from multiple clinicians, but also highlighting limitations such as visual impairment and bias due to absolute fracture stability conditions. The second research focused on evaluating callus density and size development and healing progress, correlating findings with finite element model simulations. Results indicate how callus development is influenced by bone type and fixation system, with femur cases producing larger and denser callus than tibia. Furthermore, plate fixations produced more irregular callus than nail or nail+plate treatments. FE simulations supported theories of strain-dependency of fracture healing. However, limitations related to model idealization and lack of data were noted. Finally, joint loading analysis in instrumented total knee replacements revealed linear correlations between resultant joint force, body weight, and knee varus angle. While body weight stood out as primary factor in load transmission, varus angle enhanced correlations if combined with other variables. This proves how a large amount of physiological and mechanical factors influence the load transmission at joint level and consequently at the fracture and fixation level, affecting the new bone callus' development.

1. STATE OF THE ART OF BONE FRACTURE HEALING

The hierarchical structure of natural materials, represented by collagen-based tissues in the human body, showcases a unique combination of mineral components and organic polymers. More specifically, human cortical bone demonstrates a multi-scale hierarchical organization from nano to macro levels: type I collagen and hydroxyapatite forming mineralized collagen fibrils move, at higher scales, to fibrils assembling into fibers, lamellae, and ultimately, the osteon (Fig. 1). This hierarchical organization grants exceptional mechanical properties to the bone tissue, achieving both strength and toughness. At the same time, its architecture makes the cortical bone an inhomogeneous and anisotropic material, mechanically definable as almost linearly elastic [10, 49].

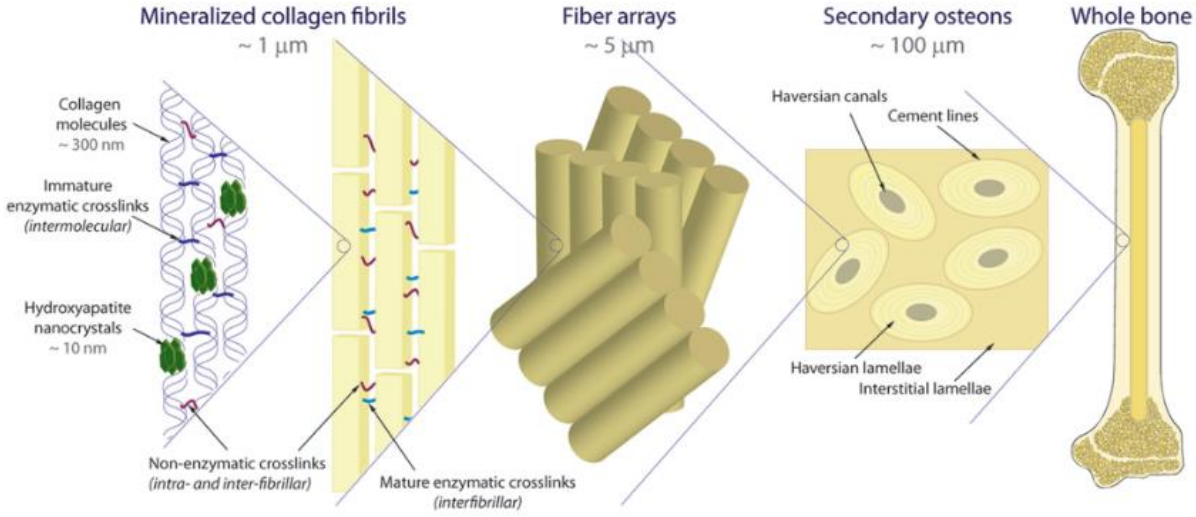

Figure 1. Hierarchical structure of human cortical bone [49].

1.1 Bone Biology

Bone tissue can grow, adapt its shape, self-repair when fractured and undergo continuous renewal processes through internal remodelling. These processes are intricately regulated by mechanical, hormonal, and physiological factors. Growth and modelling occur primarily during childhood, while fracture healing is specific to the individual fracture case.

Internal remodelling takes place throughout the entire life and it is crucial for evolution of bone microstructure, adapting structural properties, and repairing microdamage. Bone remodelling is limited to the internal surfaces of the bone matrix, where bone cells can add or remove bone tissue.

There are four types of bone cells, each with distinct functions:

- **Osteoblasts**: originated by the periosteum layer or stromal tissue of bone marrow, they can produce new bone tissue.

- **Osteoclasts**: derived from the bone marrow, they can remove bone tissue through demineralization and collagen dissolution, thanks to acid and enzymes.

- **Bone lining cells**: dormant osteoblasts that remain on the bone's surface when bone formation stops. Thanks to various stimuli they can be reactivated.

- **Osteocytes**: former osteoblasts buried within the bone matrix, residing in lacunae and able to communicate with other cells via canaliculi. They serve as mechanosensors to control bone remodelling.

It has been assumed that osteocytes, being the only cells embedded within the bone matrix, are susceptible to damage to the matrix. Microdamage, due to fatigue for example, could disrupt osteocytes' connections to the matrix, affecting communication between canaliculi or altering metabolic exchange. As a result, fatigue microdamage may initiate bone remodelling, by initially recruiting the osteoclasts.

Bone remodelling is performed by organized units referred to as "basic multicellular units" (BMUs) rather than individual cells, as coined by Frost [17]. These units operate on the periosteum, endosteum, trabecular surfaces, and cortical bone, replacing old bone with new one in well-defined sequences of activation, resorption, and formation (Fig. 2) [4].

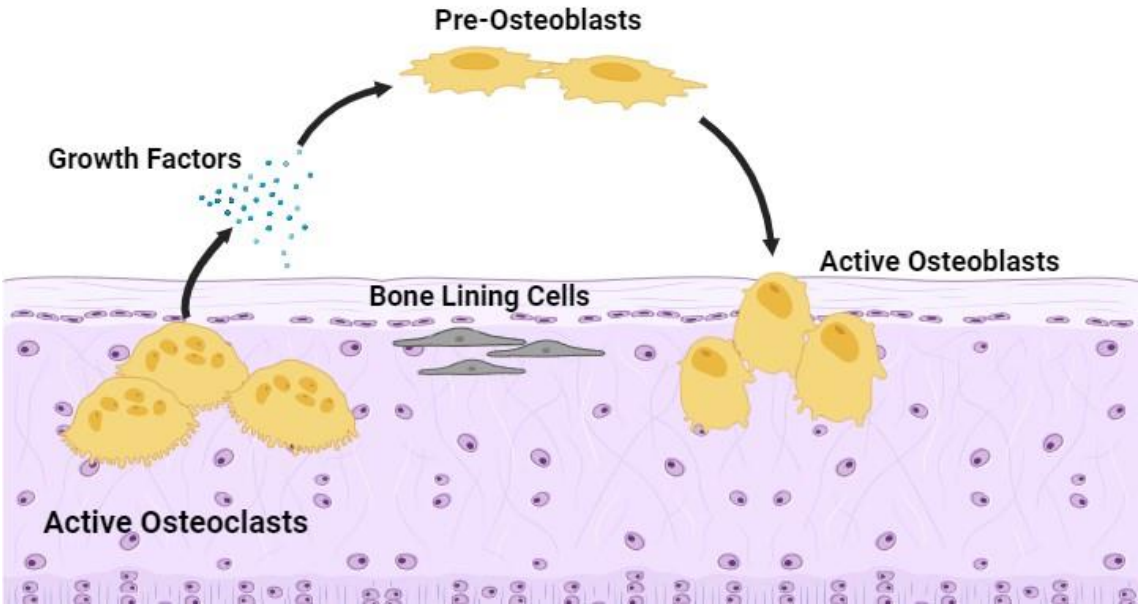

Figure 2: Activation–resorption–formation models by osteoclasts and osteoblasts [created via BioRender].

1.2 Bone fractures

Fractures can be categorized on different factors, providing valuable insights on the injury. These factors include the location, cause, shape, presence of an external wound, severity, and stability after fragment alignment. Generally, fractures can be either closed (no skin break) or open (skin break). Open fractures tend to damage surrounding tissues, with higher risk of infection and non-union compared to closed fractures. Fractures of long bones can be classified by the causing forces. Simple fractures result from a single injury, usually bending or twisting forces, resulting in two bone fragments with oblique, transverse, or spiral edges. These fractures heal naturally (Fig. 3). Instead, comminuted fractures consist in the shattering a bone into multiple small pieces, for example due to high-velocity injuries. Treating these fractures can be difficult and may lead to lasting deformities.

Stress fractures accumulate microdamage due to low-magnitude cyclic forces over time. Unlike simple and comminuted fractures, these fractures are self-repaired with bone remodelling. Unrepaired microdamage or prolonged repetitive loading can eventually lead to bone failure through microdamage propagation [4, 12].

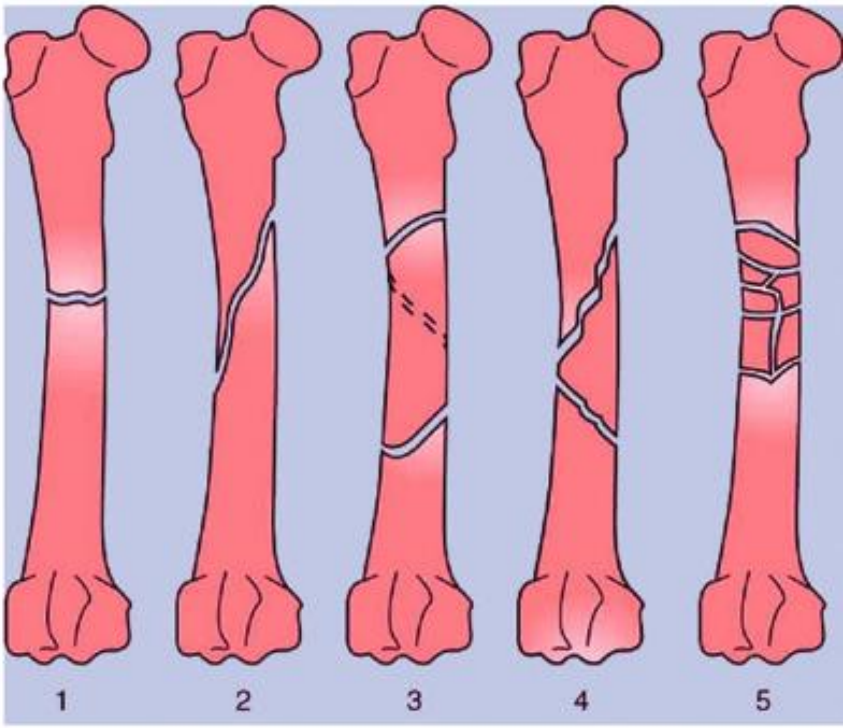

Figure 3: Types of fractures. Transverse (1), oblique (2), spiral (3), comminuted (4), multiple (5) [4].

1.3 Primary and secondary repair mechanisms

The aims of fractured long bones' repair process are restoring their anatomy and function. The process can be divided into primary and secondary healing based on the relative movement of the fracture fragments.

Primary healing typically occurs with rigid internal fixation stabilizing the fragments' alignment, concluding in direct efforts by the bone cortex to reestablish fragments' continuity. Mesenchymal stem cell-derived osteoblasts lay down osteoid on the exposed bone surfaces, provoking the reestablishment of Haversian systems across the original fracture line through intracortical remodelling.

On the other hand, secondary (spontaneous) healing is associated to a response from the periosteum and surrounding soft tissues at the fracture site. It is influenced by interfragmentary movement, inhibited by rigid fixation, and essential for bone recovery. Mesenchymal stem cells (MSCs) and osteoprogenitor cells take part in repair through intramembranous ossification and endochondral bone formation, forming new bone around the fracture site, with the contribution of osteoblast progenitor cells that synthesize new bone matrix on the surface. This process doesn't directly bridge the fracture's gap. Endochondral ossification results in the formation of a callus in the fracture site. It consists in the development of cartilage caused by the lack of blood supply and subsequent hypoxia. Chondrocytes, from MSCs in the periosteum and endosteum, undergo calcify and grow the cartilage matrix. This matrix is then replaced by the action of osteoclasts and blood vessels, followed by osteoblast-induced bone formation.

Fracture repair is notably influenced by the mechanical environment at the fracture site. Interfragmentary movement tends to favour healing through cartilage formation, while stability promotes direct bone formation. Most long bone fractures heal through a combination of both processes. Both intramembranous and endochondral ossification produce woven bone composed by a loosely organized hydroxyapatite matrix, vital for fast consolidation of fracture fragments to restore the mechanical stability. The rate of woven bone formation can be drastically faster than that of lamellar bone. Successively, osteoclasts remodel the woven bone into lamellar bone, obtaining a more organized structure [4, 15].

1.4 Stages of fracture repair

Secondary fracture healing of long bones can be considered as a series of four discrete stages occurring in sequence and partially overlapping (Fig. 5).

1.4.1 Inflammatory response

The inflammatory phase of fracture healing begins after disruption of bone and surrounding soft tissues and continues until the formation of cartilage or new bone, lasting around 3 - 4 days or longer, depending on the injury's severity. Reduction in pain and swelling are typical signs associated to this phase. Damaging medullary vessels, fractures lead to blood leakage and formation of a fibrin-rich clot in the site with hematoma, which

starts the natural healing (Fig. 5). Between various theories it has been suggested that this condition growth factors are released, able to stimulate angiogenesis and bone formation [43].

Hypoxia resulting from blood vessel disruption activates specific transcription factors, leading to shifts in cell metabolism and anaerobic energy production: platelets release growth factors to promote bone formation. Furthermore, the formation of new blood vessels is facilitated by the fracture hematoma and is mediated by factors like vascular endothelial growth factor (VEGF). Interestingly, immune cells can adapt to this harsh environment featuring low oxygen levels and dysregulated sodium and potassium levels. In fact, immune cells remain active and can produce cytokines that attract other fundamental cells for the healing process. Additionally, during these initial stages, a provisional extracellular matrix is formed which is established through the fibrin network of the coagulation process. This matrix plays as a substrate for cell adhesion and transmission of mechanical signals, essentials for early healing [16].

The new vessels generate mononuclear phagocytes, which help in the removal of necrotic bone, and contribute to the formation of the callus. They contain multiple growth factors that stimulate fibroplasia, benefiting both bone and soft tissue repair. This complex interplay of factors and cell types orchestrates the initial phases of the healing process following vascular disruption.

When medullary blood flow is restored, the extraosseous blood supply stops and the hematoma is usually resorbed within the first week, unless complications like infection, excessive motion or extensive soft tissue necrosis persist in the site [4].

1.4.2 Soft callus (cartilage) formation

In the early stages of the repair phase, capillary ingrowth, linked with mononuclear cells and fibroblasts, transforms the hematoma into granulation tissue, gaining mechanical strength (able to withstand a tensile force up to 0.1 nm/mm2) [32] and the ability to elongate up to twice its original length [37]. As granulation tissue develops or differentiates into connective tissue, collagen fibers increase in number, based on type I collagen. This tissue is organized diagonally, to optimize the elongation.

Poor vascularity and interfragmentary strain influence the development of a cartilaginous callus. In this phase, the mesenchymal cells proliferate and differentiate into chondrocytes or osteoblasts with the contribution of multiple growth factors. The periosteum thickens and becomes an external fully vascularized callus [39].

An internal callus forms within the medullary canal and it’s supplied by medullary arterioles. The presence of a layer of fibrocartilage in the canal temporarily obstacles the medullary blood flow across the fracture gap. The composition of external and internal callus constitutes the "bridging callus" (Fig. 5). This early "soft callus" resists compression but has elongation (approximately 8%) and ultimate tensile strength (4-19 MPa) like fibrous connective tissue [4].

1.4.3 Hard callus formation (endochondral ossification)

A prominent external callus is usually produced in well-vascularized unstable fractures. This phenomenon significantly increases the cross-sectional diameter of the injury site, enhancing the bending resistance and provoking an increase in strength efficiency and stiffening [32].

The higher proteoglycan concentration within the fibrocartilage is another factor that contributes to the stiffening of the interfragmentary gap: this tissue takes a fundamental part in restoring strength and stiffness, allowing the eventual formation of compact bone.

The mineralization process starts at the fragment ends and continues towards the centre, producing the "hard callus". Chondrocytes in the fracture gap control the formation of mineralized clusters while mitochondria accumulate calcium-containing granules in the site. These granules are then released in the hypoxic environment that leads to the growth of apatite's micro crystallites.

Subsequent steps in the bone substitution process are comparable to endochondral ossification [5]. The matrix compartments are degraded by macrophages and the fibrocartilage is vascularized, with blood vessels and osteoprogenitor cells forming new trabeculae. The fibrous tissue within the gap undergoes intramembranous bone formation thanks to the mechanical support from the mineralized callus and sufficient vascularity. Compact bone has an ultimate tensile strength from 100 to 200 MPa, limited elongation capacity (about 2%) and a high modulus of elasticity.

Bone union is achieved at the end of repair phase; however, the structure of the fracture site differs from the original bone (Fig. 5). The time necessary for union varies depending on factors such as location, fracture configuration, adjacent soft tissue status, and patient characteristics. At this point the injured bone regains sufficient strength and rigidity to permit low-impact exercises [32].

1.4.4 Bone remodelling

The final phase of fracture repair is focused on the morphological adaptation of bone to regain optimal strength and functions. This is a gradual process is based on the mechanical response of bone cells to stress, balancing the growth and resorption of the tissue. This phase can last between 6 and 9 years in humans, taking the most time between the four stages. In this phase, the balanced activity of osteoclastic resorption and osteoblastic deposition is guided by Wolff's law (Fig. 4) [39].

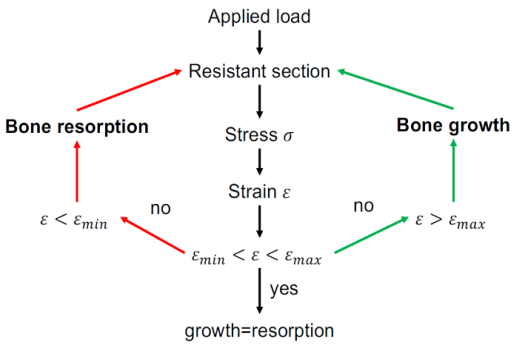

Figure 4: representative scheme of Wolff's law for bone remodelling: if the strain produced by the applied load is below the physiological range, bone resorption is initiated by osteoclasts; thinning endosteal and periosteal sides, trabeculae and/or reducing the mineralization of the matrix. If instead, the strain exceeds the range, the opposite occurs (osteoblasts act to thicken the tissue and enrich it) [10].

For a spontaneous healing, the transition from soft to hard callus depends on gradual increase in stability and adequate blood supply at the fracture site (Fig. 5). Excessive instability and compromised vascularization can cause the formation of fibrous tissue and development of atrophic non-unions. Instead, well-vascularized fractures with uncontrolled interfragmentary motion may become cartilaginous callus, insufficient to stabilize the fragments and leading to hypertrophic non-unions or pseudoarthrosis. If both blood supply and stability are achieved, the result is the formation of mineralized callus, but initial displacement of bony fragments caused by trauma and muscle contraction can frequently lead to malunion [4] (Fig. 6).

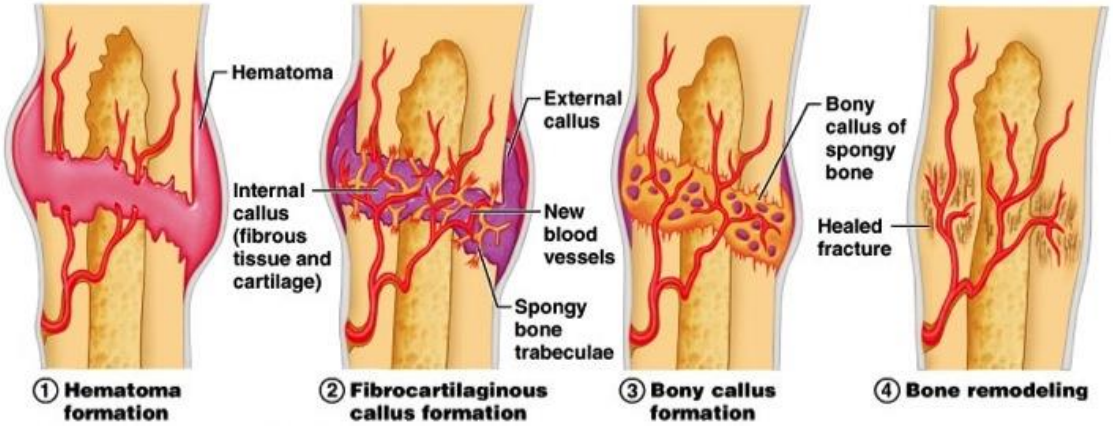

Figure 5: the four phases of bone regeneration: after the formation of hematoma in the fracture site, gradual development of fibrocartilaginous callus is followed by denser bone formation, reaching the last and longest step of remodelling [50].

Figure 6: on the left an example of tibia treated with nail fixation, the radiographic image represents the last follow-up stage, but still a not complete union is present at the diaphyseal level. On the right an analogue case, but with complete union developed.

2. TREATMENT AND ASSESSMENT OF BONE FRACTURES

2.1 Fracture classification (AO/OTA)

In 1959, a group of 13 Swiss surgeons founded the Association of Osteosynthesis (AO) with the aim of improving fracture care through standardization. In 1963, the first edition of the "Manual of internal fixation" was published and in 1986, the foundation officially adopted “The Comprehensive Classification of Fractures of the Long Bones” developed by Maurice Müller and his group [2, 25]. This system unified diverse fracture systems, providing a standardized language for orthopaedic information and it was integrated in trauma databases, scientific journals, and textbooks worldwide. Periodic revisions were performed to constantly update and optimize the system. This commitment to periodic revisions ensures the adaptation of AO/OTA classification system to the evolving landscape of orthopaedic knowledge and continues to match the needs of the orthopaedic community [51].

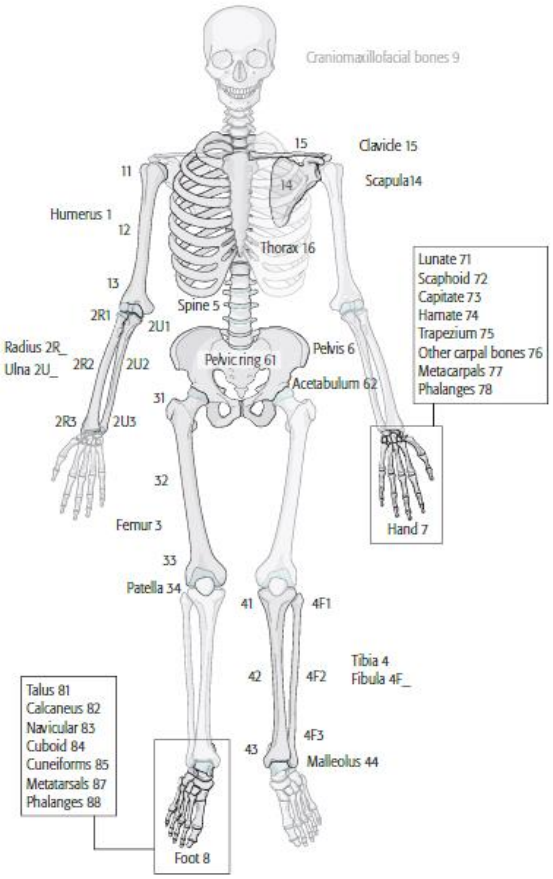

Figure 7: Design of bone location [51].

First, the bone needs to be identified (Fig. 7).
Next, it’s necessary to determine its location and it’s required to precisely define the parts of a bone. The proximal and distal ends of long bones are defined by a square whose sides are the same length as the widest part of the epiphysis/metaphysis in question (Heim’s system of squares) (Fig. 8). Each bone has a proximal and distal end segment, between which the diaphysis or shaft is located. Having separate codes for two bone systems, it was decided to maintain the standard definition of the end segments with bones not separated. Two exceptions are the proximal femur, due to being above a line passing transversely through the inferior edge of the lesser trochanter, and the malleolar segment of the distal tibia.

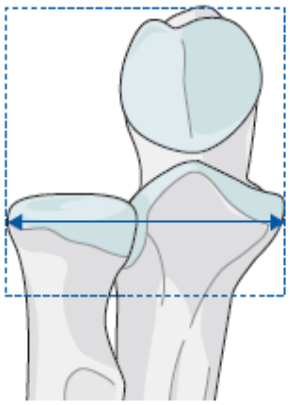

Figure 8: Determine the location of the end segment [51].

The bone segments are numbered: Proximal end segment = 1, Diaphyseal segment = 2, Distal end segment = 3.

The location of the fracture is determined by its centre. This is defined as follows:

- In simple fractures, the centre is clear (Fig 9).
- In wedge fractures, the centre is at the level of the broadest part of the wedge (Fig. 10).
- In fragmentary wedges and multifragmentary fractures, the centre can be determined only after reduction (Fig. 10).
- Diaphyseal fractures associated with a displaced articular component is considered an articular fracture.
- If the fracture is associated with an undisplaced fissure that reaches the joint, it is classified as a metaphyseal or diaphyseal fracture depending on the centre.
- If one bone has two separate fractures, one in the diaphysis and one in the proximal or distal end segments, each one must be classified independently.

The type (upper-case letter) is a general description of fracture patterns while the group (numerals) is more specific, based on the bone itself or specific fracture patterns.

The morphology of the diaphyseal fracture is defined as:

- **Simple - Type A**: fractures with single circumferential disruption of the diaphysis. An oblique fracture forming an angle bigger or equal to 30° to a line perpendicular to the long axis of the bone. (Fig. 9).

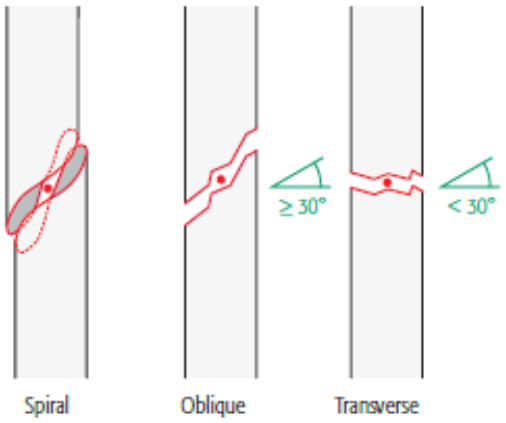

Figure 9: Simple fractures. The dot represents the fracture's centre [51].

- **Wedge - Type B**: fractures characterized by contact between the main fragments after reduction, usually restoring the normal bone's length. The wedge fragment can be intact or in multiple fragments. The difference between spiral and bending wedge is inconsistent and not easily determined, so these terms were moved to the universal modifiers (Fig. 10).

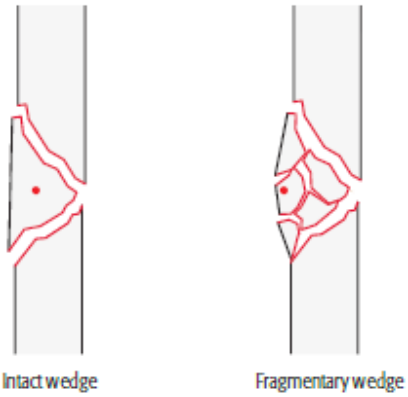

Figure 10: Wedge fractures. The dot represents the fracture's centre [51].

- **Multifragmentary - Type C**: multiple fracture fragments and lines present. In the diaphyseal segment, the fractured segment can be intact or in many fragments, so that if the fractured area were removed after reduction, there would be no contact between the proximal and distal portions. Fragmentary is used to describe fragmentation of a wedge or segment (Fig. 11).

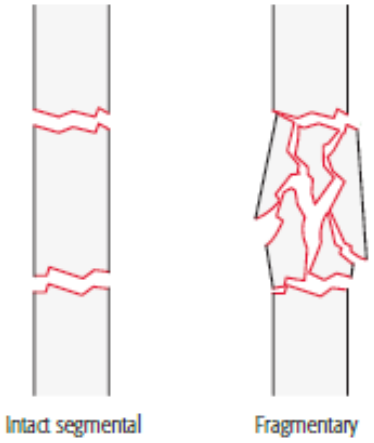

Figure 11: Multifragmentary fractures [51].

The universal modifiers are descriptive terms of fracture displacement, morphology, location, or associated injury, generalizable to most fractures, providing optional details for users. Universal modifiers may be added to the end of the fracture code within square brackets and multiple ones could be contained within the same set of squared brackets and separated by a comma (Fig. 12) [51].

This classification proved to be extremely useful to obtain a standardized and easily accessible way to communicate, analyse and correlate fracture types to bones and related traumas.

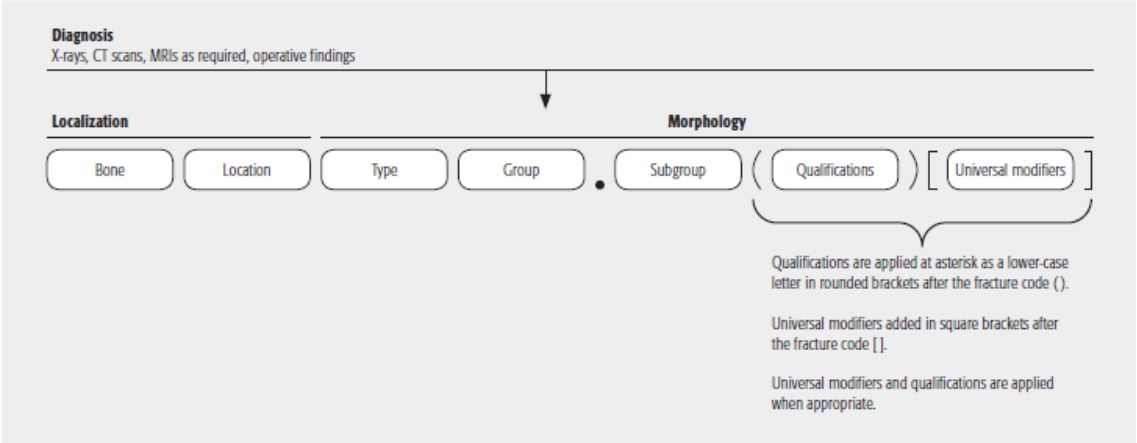

Figure 12: Alphanumeric structure of the AO/OTA classification [51].

2.2 Fracture treatment strategies

2.2.1 Fracture fixation

Wolff's law emphasizes the interlink between bone biology and mechanical loading, fundamental for bone healing [39]. However, other factors need to be assessed.

Long bone fractures, especially in the lower limbs, experience considerable forces, resulting in interfragmentary motion at the fracture site. This motion, ranging to a few millimetres, is influenced by various elements, including fracture characteristics, fixation type and configurations, and patient-related factors (Table 1)

Fracture Characteristics:	• Gap size. • Bony support under load. • Level of comminution (e.g., number and size of fragments). • Localization within the body. • Position of the fracture.
Fixation Type and Configuration:	• Position and type of fixation system. • Compression or bridging techniques (e.g., compression, neutralization, locked bridging plate). • Implant material (e.g., steel or titanium). • Implant placement.
Patient-Related Factors:	• Gait speed and leg alignment (e.g., varus/valgus). • Muscle activation and coordination (e.g., muscle damage or dementia). • Type of activity. • Walking aids and the ability to properly use them. • Weight/BMI considerations.

Table 1: factors influencing callus development in fracture patients.

The interfragmentary motion during the fracture healing process plays a crucial role, and all these factors need to be assessed to properly evaluate it [6, 14].

Choosing the most suitable approach for fracture fixation can be difficult, especially if biological constraints such as comorbidities or complex trauma are considered. AO principles have guided fracture fixation, focusing on proper stabilization for the specific cases. However, the mechano-biological consequences of these treatments aren’t always

deeply studied. The comprehension of mechano-biological interplay during tissue regeneration is crucial for fast and effective healing, especially with biological compromise and limited regenerative capacity. In such cases, a modern fracture fixation strategy aims to protect the remaining biological capacity without overstressing mechanical capabilities. It's necessary to consider at the same time the initial stabilization with immediate functional outcomes, but also a treatment that respects and supports biological healing potential [21, 31].

The right trade-off between stiffness and flexibility in fixation is a very critical point. Excessive rigidity or excessive flexibility can respectively lead to inefficient healing or non-union. Optimal healing is promoted by moderate tissue straining accompanied with minimal shear stress. Shear movements at the fracture site tend to hinder healing by blocking vascular ingrowth and affecting the transition from the pro- to anti-inflammatory phase: preserving blood supply without overburdening the mechano-biological capabilities of the tissue and the mechanical capacity of the fracture fixation is a delicate and fundamental concern [24, 38].

Differences between nail and plate fixation are minor, but complications vary. Locking plates and screws, favoured in compromised bone quality, offer advantages. Screw positioning is another fundamental factor, playing a crucial role in determining mechanical stability, with moderate in-between distances to avoid excessive swinging and shear at the gap.

At the same time newer techniques, like double-plating or locked nailing, have been exploited. Even though their effectiveness compared to conventional options is debated, it's clear the emphasis on customized fracture fixation considering patient-specific needs, based on the benefits obtained from flexible configurations for regenerative tissue deformation. These modern implants allow customization, but the interaction with local bone formation is unclear. Effective treatment requires fracture fixation supporting dynamic mineralized tissue deposition for optimal biomechanical stability [14, 21, 31, 38].

2.2.2 Cell-based therapies

Current research involves hundreds of clinical trials investigating stem cell applications in promoting bone healing. However, these treatments aren't a standard for bone diseases yet, due to several challenges. Stem cells are naturally rare in the body, while stem cell therapy consists in flooding the recipient tissue with a significantly higher number of cells; with the transplanted cells often having a short lifespan, with low efficiency in terms of integration and proliferation. Nevertheless, there is a growing interest in exosome regenerative therapy, where dying stem cells may promote healing. Additionally, fibroblasts, which are more abundant and have similarities to stem cells, are explored as potential regenerative cells with the correct signalling achieved [8, 42, 44]. Autologous bone grafting is currently the preferred method for critical fracture repair, but with still unclear factors responsible for its success. Understanding the true "modus operandi" of cell-tissue transplantation may lead to improved optimization of this approach [14].

2.3 Assessment of fracture healing

Since so many variables influence the healing process, the healthcare personnel need to periodically check-up the patients throughout the rehabilitation stages to ensure an efficient clinical outcome, keeping the fixation system stable and guaranteeing a beneficial bone restoration. This can be achieved through follow-ups set up by the surgeon and, via different fracture assessments, it's possible to evaluate the healing progress and act consequently; with worst cases consisting of even substituting / revising the fixation system if potentially needed. In some conditions, physical therapy is also necessary, with a synergetic collaboration between the trainers / physiotherapists and clinicians to provide feedback on the patient's progress, along with any possible concerns [41].

Consequently, both structural and biomechanical assessments are fundamental to evaluate the progress of fracture repair. Additionally, clinical indicators are crucial for monitoring healing stages in a non-invasive manner.

- **Structural Evaluation**:
  Assessments involving methods like radiography and histology. Radiographic evaluation is a widely employed technique in both laboratory and clinical settings. The Radiographic Union Score for Tibial fractures (RUST) was developed to evaluate radiographic fracture healing, particularly for intramedullary nail fixation. Whelan et. al [48] aimed to establish the RUST score's reliability and validity compared to existing scoring systems, discovering that quantification of cortical continuity by counting the number of cortices with bridging callus or a visible fracture line was more reliable than other techniques. The score is determined by the absence of callus (1 point), visible fracture line (2 points) or presence of callus without visible fracture lines (3 points) on each of four cortices on antero-posterior (A-P) and medio-lateral (M-L) radiographic images (Table 2). Cekic et. al [7] conducted a patient-based retrospective investigation, considering both the clinical properties of patients and clinical evaluation scales, discovering that RUST scores were directly related to patients' clinical conditions. High pain scores were correlated to unclear callus bridging in two or three cortices and/or disappearance of fracture line on X-ray images. The RUST scoring system was considered accurate to detect both radiological and clinical union problems in tibial bone fractures, suggesting using the system from the preoperative period and collecting data until fracture consolidation to obtain more accurate results. Initially the RUST scoring system was developed for tibial fractures; it was considered valuable for other long bones, with the additional necessity to standardize with respect to bones' dynamics during fracture union. Still there was no value defining union and no validation for metaphyseal fractures or those treated with plate fixation treatments.
  Litrenta et. al. focused [29] on a study to assess the reliability and define radiographic union in the context of tibia and femur fractures, particularly in the diaphyseal region, treated with plates or intramedullary nails. Trauma surgeons evaluated radiographs with a modified RUST, exploiting criteria such as callus formation, cortical continuity, and bridging. Successively, radiographic results of multicentre trials were reviewed at various time points, comparing plate and nail fixation, with the modified RUST score employed. The correlation between

radiographic healing and clinical outcomes was analysed, proving higher reliability with respect to the standard RUST score. This improved scoring system, especially when used in conjunction with clinical evaluation, could provide valuable insights into the healing process, offering a useful tool for orthopaedic practice. In the present time, the modified Radiographic Union Score for Tibia fractures (mRUST) scoring system is a validated metric to evaluate fracture's healing. The system assigns values from 1 to 4 for each cortex. The score is determined by the absence of any callus (1 point), callus with visible fracture line (2 points), callus showing bridging (3 points) or presence of remodelled callus (4 points) on each of four cortices on antero-posterior and medio-lateral radiographic images (Table 2) [9]. The mRUST scores are added together, ranging from 4 to 16. This system was found to prove slightly higher intra-class correlation coefficients than RUST and it has been shown to correlate with mechanical stiffness estimates [1].

	Radiographic Criteria		
	Callus	**Fracture Line**	**Score***
RUST	Absent	Visible	1
	Present	Visible	2
	Present	Invisible	3
mRUST	Absent	Visible	1
	Present	Visible	2
	Bridging	Visible	3
	Remodeled	Invisible	4

Table 2: RUST and mRUST rating specifications [9].

- **Biomechanical Evaluation**:
  Assessments involving mechanical tests like torsion and four-point bending. The choice between these tests depends on technical considerations. Torsion testing is preferred as it subjects each cross-section of the callus to a uniform torque, ensuring consistent evaluation. Conversely, four-point bending may create non-uniform bending moments throughout the callus, leading to potential results that don't highlight the weakest cross-section of the callus. It's noteworthy that three-point bending is not recommended for estimating the mechanical properties, especially during the early stages, as it applies force to the original fracture line, which may primarily consist of less mature bone tissue, cartilage or calcified cartilage, depending on the healing stage. The outcome measures obtained from mechanical tests, such as stiffness, ultimate strength, energy to failure, and torque in the torsion test, primarily reflect structural properties rather than material ones [36].

The results obtained can prove the reliability of the callus development and highlight or not the natural process of restoring normal mechanical characteristics of bone tissue in the fracture site.

- **Morphological Evaluation**:
  Another methodology, usually exploited in a laboratory environment, involves light microscopy. It's the most used technique for morphological evaluation and permits histomorphometric measurement of various parameters on the healing stages on animal specimens. This includes assessing callus size, mineralized and cartilaginous volumes, bone cortex, marrow cavity areas and cell constituents [28]. The histopathological examination is often scored based on systems like Emery's, categorizing healing outcomes from an empty gap (score 0) to complete filling with bone (score 7) [5].

- **Advanced Techniques**:
  These techniques include MRI, microCT scans, microcomputed tomography angioscans and telemetric implants, which are gaining significance in assessing bone healing quality in both in vivo studies and clinical practice, providing additional insights into bone volume and densitometry. [3, 34, 35].

In summary, fracture healing assessment is a multifaceted process which integrates biomechanical, morphological, radiographic and histological techniques, with advanced imaging methods playing an increasingly prominent role in research and clinical applications.

2.4 Objective of the study

The thesis focuses on the necessity to improve the understanding of the fracture fixation influence on bone healing processes. First, a study concerning the validity of mRUST scoring system on a clinical database will be presented to visually detect the fracture healing process with different fixation treatments and understand how clinicians face possible challenges with radiographic fracture images via inter-observer variability parameters. Then, a study based on the same cohort will focus on quantifying the size and density of callus developed, to comprehend how fixation treatments affect the new bone callus and correlate the results with finite element models. Finally, a study focused specifically on joint loading analysis will provide additional insights on further variables influencing the bone healing in the fracture site.

3. RADIOLOGIC IMAGE ANALYSIS OF FRACTURE HEALING

Long bone fractures represent a significant challenge for determining the best and most efficient treatment strategies to efficiently stimulate bone healing and an adequate bone callus. At the same time, there is no universal assessment of end point for bone healing phase post-treatment. The complexity can be related to both the diverse nature of such fractures and the need for precise and patient-tailored care. These fractures are influenced by numerous variables (e.g., type, age, fracture location, health state). Additionally, the availability of different treatment options (nail, plate, external fixators etc…) further complicates the decision-making process and it's fundamental considering physiological factors such as the patient's overall well-being, fracture stability and potential joint involvement. Considering all these factors, finding a universal and validated way to rate and assess the end point of the bone healing process is challenging [13, 16, 27, 33]. The mRUST scoring system has proven valuable insights on the bone callus' quality and can be considered as a good indicator for assessments on fracture healing [9].

The objective of this part of the thesis was validating the mRUST score as reference to the end point of the healing phase (Table 1) and judge if it's possible to provide suggestions on the most efficient treatments for specific fracture fixation options [22].

3.1 Materials and Methods

3.1.1 Subjects

The retrospective analysis included patients aged 18 years or older who underwent surgery for an extra-articular long bone fracture (femur or tibia) between January 2005 and April 2022 at Charité Universitaetsmedizin Berlin, Germany, Ethic board approval EA4/099/22. Inclusion criteria required patients with X-rays on antero-posterior and medio-lateral planes with at least one follow-up time point.

Exclusion criteria were applied to patients with various critical clinical conditions at the time of the operation (e.g., unstable circulatory conditions, surgical ineligibility, or lack of treatment consent), pregnant and lactating patients, individuals lacking legal competence and patients with fractures involving joint articulations. Cases with insufficient imaging data quality and inadequate documentation, were also excluded.

Six experts participated in the study with various years of experience in radiographic and orthopaedic fields (7.5 ± 2.6 years).

A total of a hundred and sixty-six patients were included for analysis and constituted the database of radiographic images for the study (Table 3).

	All patients (n=166)	Femur (n=63)	Tibia (n=103)
Sex	112 M (67.47%) 54 F (32.53%)	43 M (68.25%) 20 F (31.74%)	69 M (66.99%) 33 F (32.04%)
Age	43.4 (SD: 15.75; 18-84)	41.22 (SD: 16.68; 18-84)	44.73 (SD: 15.09; 18-78)
Weight (kg)	81.41 (SD: 15.81)	80.03 (SD: 15.85)	82.13 (SD:15.87)
Height (m)	1.76 (SD: 0.09)	1.74 (SD: 0.09)	1.77 (SD: 0.08)
Side	87 R (51.2%) 79 L (47.59%)	34 R (53.97%) 29 L (46.77%)	53 R (51.46%) 50 L (48.54%)
Trauma	122 high-energy (73.49%) 44 low-energy (26.51%)	56 high-energy (88.89%) 7 low-energy (11.11%)	66 high-energy (64.08%) 37 low-energy (35.92%)
Fixation	103 Nail (62.05%) 42 plate (25.3%) 18 Nail+Plate (10.84%) 3 Other (1.81%)	44 Nail (69.84%) 16 Plate (25.4%) 1 Nail+Plate (1.59%) 2 Other (3.17%)	59 Nail (57.28%) 26 Plate (16.5%) 17 Nail+Plate (16.5%) 1 Other (0.97%)

Table 3: Patient's cohort for the study. A total of 166 patients, 63 patients with femur fractures and 103 patients with tibia fractures. Groups showed comparable characteristics regarding physiological variables; however, femur fractures are more often caused by high energy trauma. In both groups, nail fixation was the most common treatment.

For the analysis with mRUST scoring system, multiple digital documents were prepared. Each case consisted in patient number, follow up stage and bone type. Furthermore, dual images were available to rate simultaneously the anterior and posterior cortices with the sagittal plane and then medial and lateral cortices with the frontal plane (Figure 13).

For all images, raters were asked to rate the callus from 1 to 4 and the "N/A" option was available in case it wasn't possible to correctly see and rate the image (Figure 13).

In the condition of assessing multi-fragmentary cases, clinicians were able to score the proximal fracture first and then the distal one, by simply assessing the same images on the dual plane twice (once for each fracture).

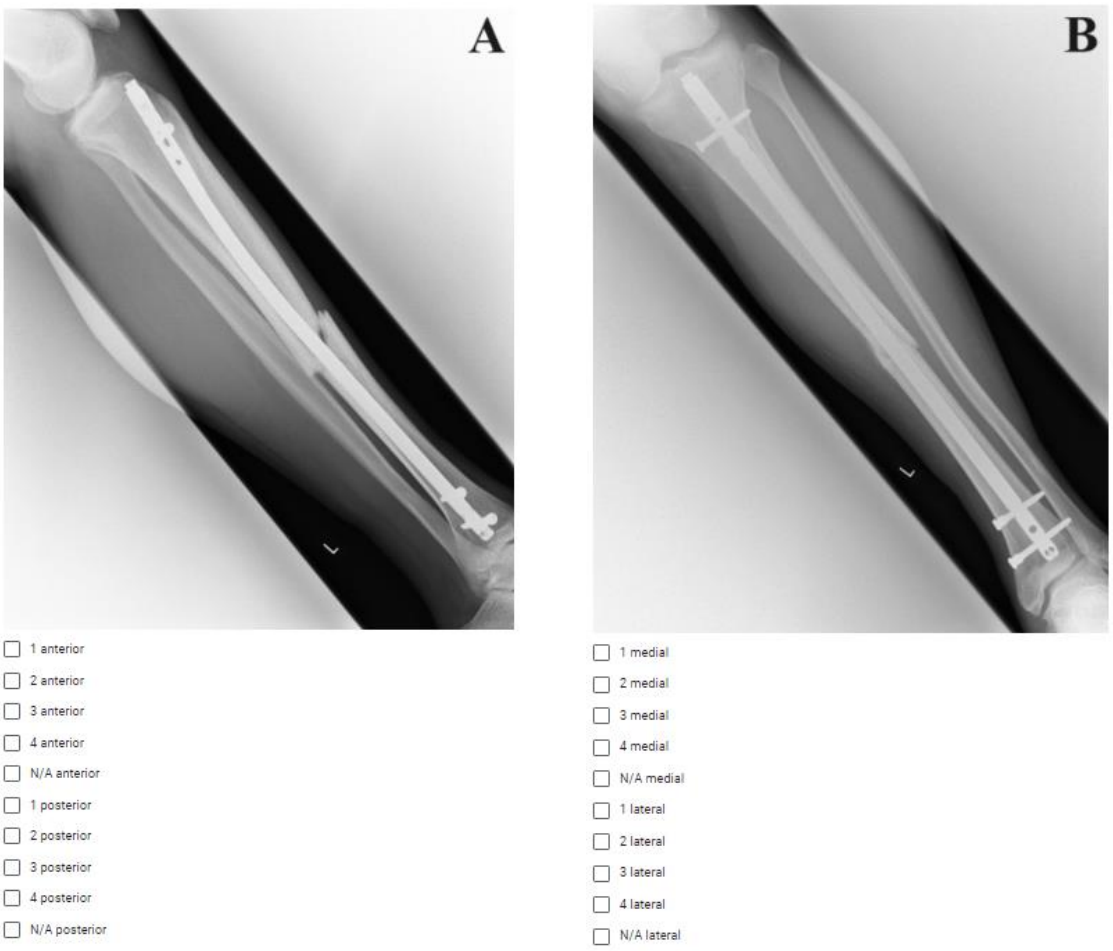

Figure 13: example of document section in which it was possible to rate simultaneously antero-posterior cortices (A) and medio-lateral ones (B). It's clear the need to assess fractures on both planes, since fracture's displacement is largely different from different point of views and so the fracture evaluation.

3.1.2 Preliminary Analysis

Once all scores were collected, a preliminary analysis was performed. A total of 1136 cases were present in the database (concerning all the patients and relative follow-up stages). From these, 7 missed the antero-posterior view and 38 the medio-lateral one. Considering that each case was based on images on both planes, the total amount of available radiographic images was 2227 (1129 images on A/P plane and 1098 on M/L plane). Intraoperative and fluoroscopic images present in the dataset were excluded from the analysis.

First, for each cortex side and case, if the majority of ratings from clinicians consisted of "N/A", the case itself was excluded from further analysis due to overall inability to properly assess the callus on that specific image (Table 4 and 5).

Impairment Analysis

Cortex side	anterior	posterior	medial	lateral
Nr. Unavailable images	111	46	40	50
% Available images	90	96	96	96

Table 4: analysis of unavailable images for each cortex and consequent percentage of available ones. It's clear how most cases improperly assessable are on the anterior side, while on the other portions the values are overall similar.

	Impairment's cause				**% Impairment's cause**			
Type	anterior	posterior	medial	lateral	anterior	posterior	medial	lateral
Plate	110	35	39	49	10.02	3.19	3.45	4.34
Nail	0	1	0	1	0.00	0.09	0.00	0.09
Nail + Plate	0	10	0	0	0.00	0.91	0.00	0.00
Plate + External Fixator	1	0	1	0	0.09	0.00	0.09	0.00

Table 5: in-depth study of the impairment's causes and related influence on the overall dataset. It's proven how plate treatment largely influenced the scoring of the cortex on all its portions, with notable effect on anterior callus. Other treatments showed less concerns and specifically the impairment caused by nails was almost irrelevant.

All the remaining cases were sorted with respect to the cortex side, to evaluate the Intraclass Correlation Coefficient (ICC) for each portion of the callus. Additionally, the same analysis was performed on the mRUST total score (summing the scores from all cortices).

Considering the condition in which the minority of experts rated the fracture "N/A" a further filtering has been performed. If individual anomalies were found in the dataset (all experts rated the callus side except one) the missing value was added as the mean of the other ones, otherwise the entire case was ignored. This permitted preserving useful data, without losing a relevant number of cases.

Single N/A assessment

Cortex side	**Anterior**	**Posterior**	**Medial**	**Lateral**
Number of cases	958	1029	1052	1052
Anomalies	32	52	32	67
% Anomalies	3.34	5.05	3.04	6.37

Table 6: Anomalies were defined as conditions in which all experts except one rated a specific cortex. To avoid ignoring all ratings for that specific case and losing useful data, the missing score was added as the mean of the other ones.

ICCs for each cortex were calculated on the entire dataset (ignoring the bone type and treatment), with respect to the bone, with respect to the fixation, and the relevant combinations bone-fixation (tibia-nail, tibia-plate, femur-nail, femur-plate). Analysis on Nail+Plate and Plate+External fixator cases were ignored due to the lack of sufficient data.

3.2 Results

First, the dataset gave the possibility to visually evaluate the healing process on different bones and fixation treatments. Example cases of callus development are shown (Figs. 14, 15, 16) to demonstrate how each healing process is different and can be determined by numerous factors, such as initial trauma, bone type, fixation treatment, physiological response.

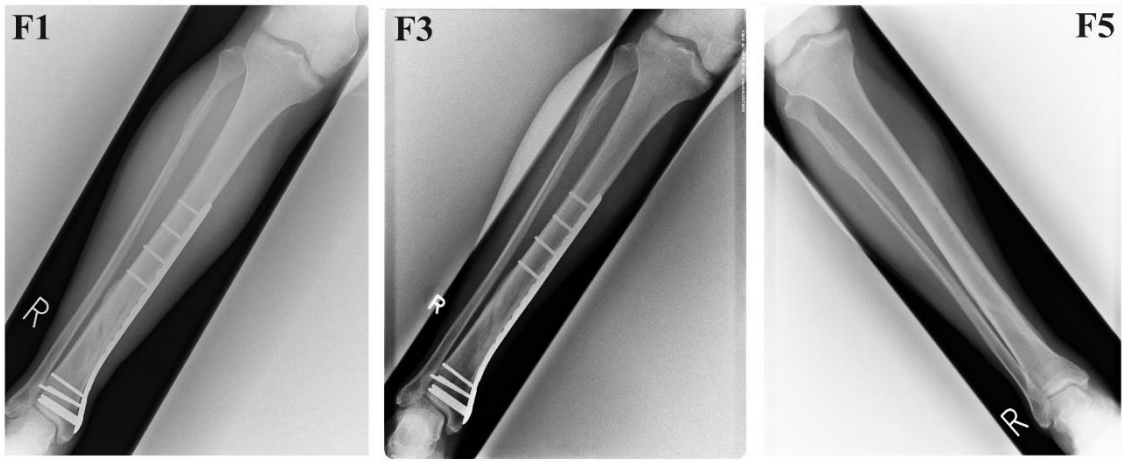

Figure 14: Patient 6 treated with plate fixation on the tibia during follow-up stages F1 (approx. two weeks post-surgery), F3 (approx. six months post-surgery) and F5 (approx. ten months post-surgery). Here it's possbile to note how the callus is homogenously distributed on the site.

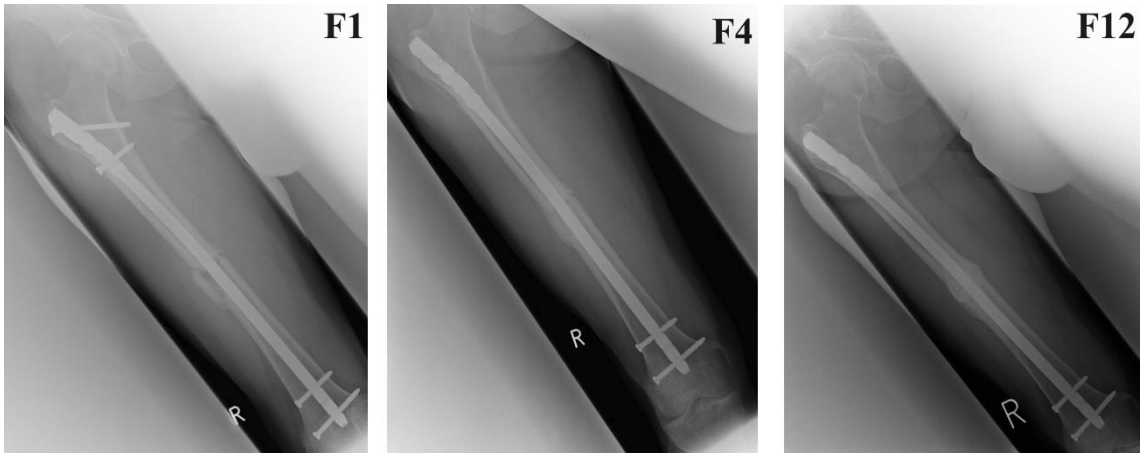

Figure 15: Patient 27 treated with nail fixation on the femur during follow-up stages F1 (approx. a month post-surgery), F4 (approx. six months post-surgery) and F12 (approx. twenty months post-surgery). On the femur the resulting callus is usually different, with more prominent bulging and more follow-up stages needed to reach an appreciable new bone development.

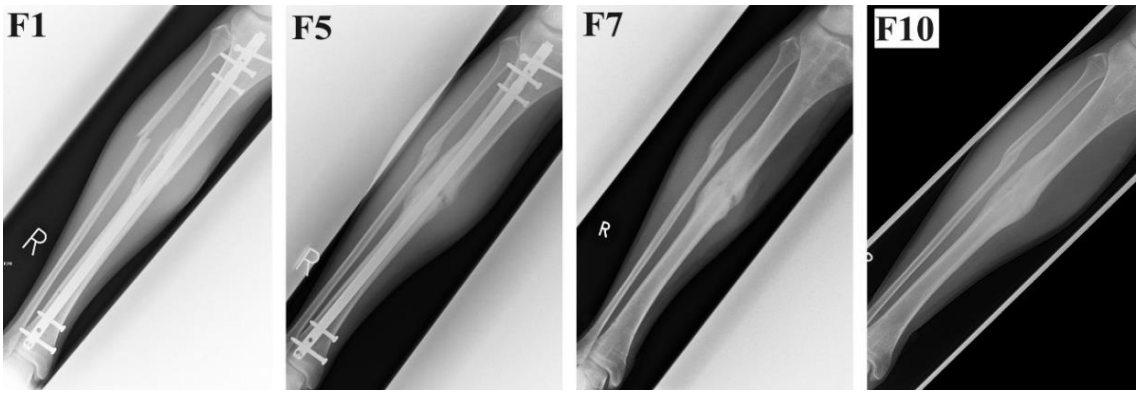

Figure 16: Patient 130 treated with nail fixation on the tibia. F1 (approx. two weeks post-surgery), F5 (approx. seven months post-surgery), F7 (approx. eight months post-surgery) and F10 (approx. twenty months post-surgery). This case shows a larger initial trauma, with more prominent fracture and an additional one on the fibula. The final callus, larger, less homogeneous and developed lately with respect to figure 18 proves how each case depends on various factors.

Intraclass Correlation Coefficients (ICC)

Cortex side	Anterior	Posterior	Medial	Lateral
Overall	0.71	0.68	0.74	0.71
Nail (overall)	0.73	0.70	0.75	0.75
Plate (overall)	0.66	0.66	0.71	0.63
Tibia (overall)	0.70	0.67	0.74	0.70
Tibia - Nail	0.73	0.69	0.76	0.74
Tibia - Plate	0.64	0.65	0.70	0.60
Femur (overall)	0.74	0.72	0.73	0.75
Femur - Nail	0.73	0.74	0.72	0.74
Femur - Plate	/	0.65	0.73	0.71

Table 7: Intraclass Correlation Coefficient for each cortex side, considering the overall data, only the nail cases, only the plates, only tibias, only tibias with specific treatments and the same for femur (missing value in femur cases treated with plates reflects the lack of sufficient data).

Analysis on the overall mRUST was performed to evaluate any deductible variations between analysing the specific cortices or the overall callus development (Table 8).

Intraclass Correlation Coefficients (ICC)

	mRUST
Overall	0.77
Nail (overall)	0.79
Plate (overall)	0.79
Tibia (overall)	0.77
Tibia - Nail	0.78
Tibia - Plate	0.77
Femur (overall)	0.81
Femur - Nail	0.80
Femur - Plate	/

Table 8: Intraclass Correlation Coefficient for each cortex side, considering the overall data, only the nail cases, only the plates, only tibias, only tibias with specific treatments and the same for femur (missing value in femur cases treated with plates reflects the lack of sufficient data).

The resulting scores highlighted the different influence of fixation treatments. Considering the overall ratings (ignoring bone and treatment), highest ICC was found in the medial cortex (0.74) with respect to the other portions, with lowest value at the posterior cortex (0.68). Same discussion can be made on overall nail cases (ignoring the bone) with highest value of 0.75 medially and laterally and lowest of 0.70 posteriorly, on overall tibia and tibia-nail cases (with respectively highest ICCs of 0.74 and 0.76 and lowest 0.67 and 0.69). Overall plate and tibia-plate cases showed highest values still in the medial callus (respectively 0.71 and 0.70) and lowest laterally (respectively 0.63 and 0.60). All femur cases showed highest ICC laterally (overall 0.75, nail 0.74, same also posteriorly, and plate 0.71) while the lowest, respectively on the posterior cortex for overall femur at 0.72, medially at 0.72 for femur-nail and posteriorly for femur-plate case at 0.65.

ICCs related to nail treatments produced better results in any category and for all cortices (overall treatment and bone type) with respect to the plate. Analysis on the anterior cortex of femur plate fixation wasn't included, due to the lack of sufficient data, producing unreliable statistical results.

ICC values based on the overall mRUST (composed by the sum of the ratings on all four cortices) showed slightly higher values on all categories. Overall femur and femur-nail cases produced the highest ICCs (respectively at 0.81 and 0.80, while lower values were found on overall case (lowest at 0.77) and tibia and/or plate cases).

Anatomic reduction is a specific condition of the fracture in which the callus could be unexpected, or the fracture line isn't visible. These clinical cases can be a relevant bias element in the results' analysis since the raters could score the fracture 1 (if they interpret it as callus absence) or directly 3 or 4 (supposing that the fracture line isn't visible anymore due to the healing process). For this reason, since a specific tester significantly differed in the scores produced regarding this concern (Table 9), the ICC analysis was performed again without its contribution to verify the bias hypothesis (Tables 10 and 11). More specifically, the related scores tended to be higher (frequently around 3 or 4, while the others rated 1 or 2).

Score recurrence assessment

Tester #	1	2	3	4	5	6
Score 1 (%)	13.45	29.49	24.36	31.69	15.80	5.68
Score 2 (%)	31.82	20.27	19.10	18.16	31.10	10.56
Score 3 (%)	25.37	28.26	24.41	19.74	26.36	44.21
Score 4 (%)	21.13	17.06	22.16	21.70	20.07	31.91

Table 9: Recurrence percentage for each score and tester has been performed to verify if there were any specific variations. The sixth rater, despite having similar year of experiences, tended to rate all fracture cases higher than the others, with lower amount of 1/2 and more of 3/4.

Post-removal biased rater				
Intraclass Correlation Coefficients (ICC)				
Cortex side	**Anterior**	**Posterior**	**Medial**	**Lateral**
Overall	0.79	0.79	0.83	0.81
Nail (overall)	0.81	0.80	0.83	0.83
Plate (overall)	0.75	0.78	0.83	0.76
Tibia (overall)	0.79	0.79	0.84	0.81
Tibia - Nail	0.82	0.80	0.84	0.83
Tibia - Plate	0.74	0.78	0.84	0.74
Femur (overall)	0.79	0.79	0.81	0.81
Femur - Nail	0.78	0.79	0.79	0.80
Femur - Plate	/	0.78	0.83	0.83

Table 10: Intraclass Correlation Coefficient for each cortex side, considering the overall data, only the nail cases, only the plates, only tibias, only tibias with specific treatments and the same for femur (missing value in femur cases treated with plates reflects the lack of sufficient data). This time without the contribution of the "biased" tester.

Post-removal biased rater	
Intraclass Correlation Coefficients (ICC)	
	mRUST
Overall	0.87
Nail (overall)	0.88
Plate (overall)	0.90
Tibia (overall)	0.87
Tibia - Nail	0.88
Tibia - Plate	0.89
Femur (overall)	0.87
Femur - Nail	0.86
Femur - Plate	/

Table 11: Intraclass Correlation Coefficient for each cortex side, considering the overall data, only the nail cases, only the plates, only tibias, only tibias with specific treatments and the same for femur (missing value in femur cases treated with plates reflects the lack of sufficient data). This time without the contribution of the "biased" tester.

The results highlighted the possible influence of anatomic reduction on the mRUST scoring system. Values increased for all categories, reaching values similar to the literature ranging from 0.75 (overall plate) to 0.82 (tibia with nail) for anterior cortex, from 0.78 (tibia with plate) to 0.80 (overall nail and tibia with nail) for posterior cortex, from 0.79 (femur with nail) to 0.84 (all tibia categories) for medial cortex and from 0.74 (tibia with plate) to 0.83 (overall nail and femur with nail) for lateral cortex.

Increments were found also for the overall mRUST scores, with lowest ICC at 0.86 for femur treated with nail and maximum of 0.90 for overall plate, reaching values similar to the literature [1,29].

Furthermore, percentage variations between pre and post results were evaluated to assess which cases were most influenced or not (Table 12 and 13).

ICC variation (%) post - tester removal

Cortex side	**Anterior**	**Posterior**	**Medial**	**Lateral**
Overall	12.24	15.65	12.20	13.67
Nail (overall)	10.89	12.97	10.63	10.83
Plate (overall)	14.51	18.96	17.87	20.91
Tibia (overall)	13.53	17.21	12.71	15.35
Tibia - Nail	12.28	15.06	10.97	12.15
Tibia - Plate	15.24	19.82	19.43	23.83
Femur (overall)	5.94	10.39	10.74	8.45
Femur - Nail	5.58	6.97	9.40	7.51
Femur - Plate	/	18.68	14.52	17.19

Table 12: percentage variation of ICC post removal of "biased" tester for each cortex. All values proved to be higher after this further analysis, specifically plate treatments on all cortices.

ICC variation (%) post - tester removal

	mRUST
Overall	12.89
Nail (overall)	11.54
Plate (overall)	14.95
Tibia (overall)	14.22
Tibia - Nail	12.81
Tibia - Plate	16.25
Femur (overall)	7.31
Femur - Nail	7.52
Femur - Plate	/

Table 13: percentage variation of ICC post removal of "biased" tester for overall mRUST. Similar trend to table 11.

Percentage variations proved again how the inter-observer variability increased on all categories and specifically on plate treatments. Highest increases were found on all cortices for overall plate, tibia-plate and femur-plate (anteriorly 14.51% overall, 15.24% tibia-plate; posteriorly 18.96% overall, 19.82% tibia-plate, 18.68% femur-plate; medially 17.87% overall, 19.43% tibia-plate, 14.52% femur-plate and laterally 20.91% overall, 23.83% tibia-plate, 17.19% femur-plate). Lowest variations were related to femur-nail cases, which were already properly assessed and visually easier to evaluate.

3.3 Limitations and Discussion

From the results obtained, it can be noted how most cases excluded from the study were related to plate fixation. Furthermore, lowest values of ICC were found on plate treatments reflecting a larger spectrum of scores, proving the difficulty in conforming to the same fracture's evaluation. This was specifically highlighted by the analysis on the specific cortices, since on the overall mRUST these divergences weren't as clear.

Posterior cortices were related to the lowest ICCs. This could be explained by the difficulty to correctly visualize and assess the callus when the plate's structure covers the fracture edge, which is a relevant limitation in analysing the bone callus. This problem was also confirmed by the low lateral ICCs in plate cases. Also, the presence of fibula in tibia cases could have influenced the correct visualization of the posterior cortex.

ICC values based on total mRUST ratings proved to be higher than the specific assessments for each callus side. This could be explained by various reasons:

- Summing the cortices' scores produces a composite measure. This could have led to a reduction in the variability between testers because the scores for individual cortices might offset each other, leading to a more consistent overall rating.
- Even if the testers differed in scoring individual cortices, their consistency in the overall assessment could have contributed to higher ICC values when aggregating scores.

Radiographic images weren't always related to the same angle of the fracture, causing a possible bias effect on the resulting scores and link to problems faced on posterior and lateral cortices (specifically with plates) (Fig. 14).

Further analysis regarding anatomic reduction conditions highlighted its strong influence on this scoring system. Removing a biased tester who was more prone to rate fractures 3/4 rather than 1/2 in the first follow-up stages increased all the ICC values, specifically on plate treatments as they were also the most difficult to evaluate. This represented one of the main limitations of the mRUST scoring system: if a clinician supposes to not see any callus, due to fracture being in the first stages, the rating is low. However, the same condition can be interpreted as complete healing due to the absence of fracture line. This bias affects all the follow-up stages of that patient (if a clinician starts from 1 and doesn't see progress, scores remain low, if starts high remains with high values).

Documents' sections were organized with respect to the patient and follow-up stage, in this way experts rated the same fracture progressively during the healing process. This could have produced a bias effect on the tester which naturally expected to rate the cases in a progressive way, adding a decisional factor on the overall results. This limitation is mostly relevant considering the validity of mRUST scoring system, while in real-life cases, clinicians face situations similar to the structure of the digital forms (consequently analysing the progression of fracture healing). Excluding this bias by randomisation would exclude an existing bias in clinical practice.

Nonetheless, resulting ICCs proved good reliability on all cases, demonstrating how the mRUST scoring system is a valid asset to evaluate the progression of the healing fracture.

4. CALLUS SIZE AND DENSITY DEVELOPMENT AFTER LOWER-LIMB FRACTURE FIXATION

As previously cited, multiple fixation techniques have been developed to treat long bone fractures. However, despite the technological progress, these treatments frequently develop asymmetrical and inconsistent bone callus after surgery. So, the relationship between the specific biomechanics of the fixation system and its influence on the fracture site during healing is a relevant concern [6, 30]. Besides physical examination, X-ray is used to monitor fracture healing in clinical practice, allowing to highlight callus and fracture line. However, callus size or callus density aren't usually reported, and they can largely vary between bone localisation, size, and density, during the healing process. mRUST scoring system can be exploited to monitor the healing phases, but the factors just cited would be ignored. These parameters might give further information about the mechanical forces or the local deformation of regenerative tissue that stimulates fracture healing.

The specific callus size and density during follow-up could be used to better delimit the exact thresholds of beneficial and detrimental tissue deformation for osteogenic healing. Aim of this study [11] was evaluating callus size and density of lower-limb fracture with a biomechanical model to correlate biomechanical stress and strain with the radiographic appearance of bone healing.

4.1 Materials and Methods

4.1.1 Subjects

The retrospective study was based on the same dataset of chapter 3 (see Table 3).

4.1.2 X-ray assessment

Callus size, callus density and fracture healing progress were assessed using the region of interested tool (ROI) "closed polygon" in a DICOM-viewer "Horos" [11] (Fig. 17) by a radiologist with 3 years of experience in musculoskeletal imaging. The reader was blind to clinical data, timepoints and outcome.
Callus-sizes were measured at each cortical site (medial, lateral, ventral, dorsal) for all available images. Bone shafts were assessed at the middle shaft and were used for size normalization:

- **normalized callus size**: callus area (in cm2 in planar X-ray)/ callus width (in cm).

The mean density of each measured callus was determined, placing the region of interest at the lateral/ ventral cortex in the upper third of the bone shaft and was used for normalization:

- **normalized density**: ROI callus/ ROI cortex.

The modified union score for tibia fractures (mRUST) was assessed by rating callus formation and fracture line (ranged from 4-16) for each timepoint. To compare at comparable follow-up times, specific time points T1-T4 were chosen for evaluation (T0:

0 (+45) days post-surgery; T1: 90 (± 45d) days post-surgery, T2: 180 (± 45d) days post-surgery, T3: 365 (± 45d) post-surgery, T4: 730 (± 45d) days post-surgery).

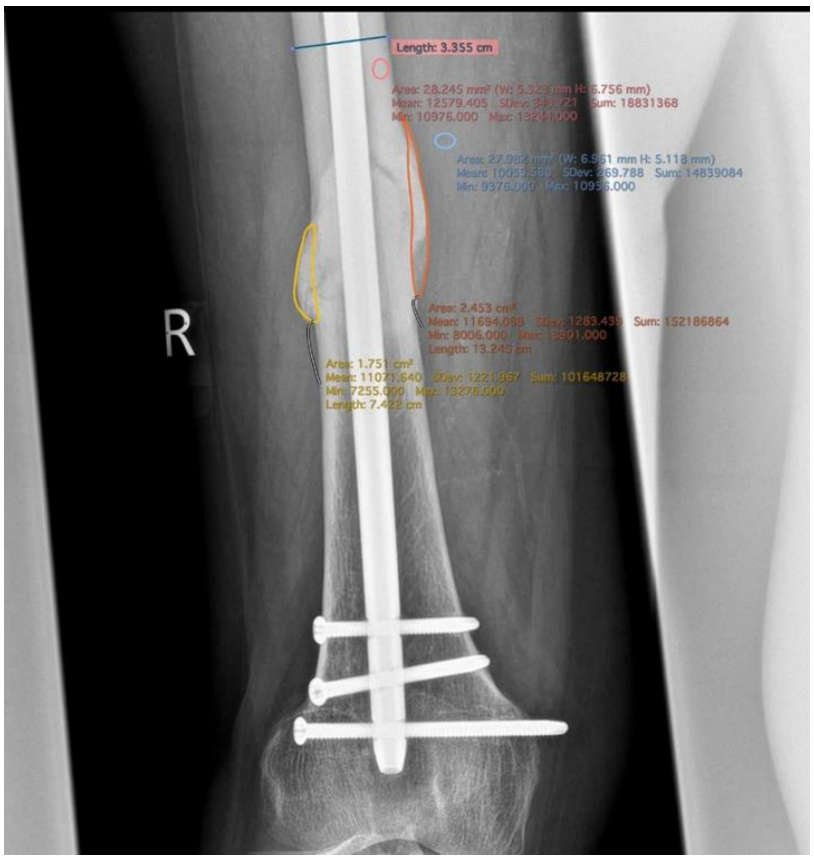

Figure 17: Relative callus size and density evaluation for a femoral shaft fracture stabilized with an intramedullary nail: callus width identified at femur shaft (blue line), medial (red zone) and lateral (yellow zone) cortices.

4.1.3 In silico model

Four idealized finite element (FE) models were created to quantify the approximate mechanical stimulation of healing (deformation at the fracture site). Two femurs and two tibias, fixed with plate or intramedullary nail. A mid-shaft 5mm transverse fracture model was implemented. Mechanical boundary conditions were roughly matched to clinical cases concerning the covariates of bone loading (femoral or tibial load during walking from Heyland et al. [23], Table 15), and idealized fracture fixation implant. The modelled implants were a locking plate (300mm length, 20mm width, 3mm thickness) or an intramedullary nail (300mm length, 10mm diameter). For both fixations, only one proximal and one distal bi-cortical locking screw (5mm diameter, bridge span: 237.5mm) were modelled as rigidly fixed to bone (200mm length per bone fragment, 405mm total length 2.5mm cortical thickness) and plate or nail, i.e. the interface between screw and bone/implant didn't allow relative motion (tied). Implants were modelled from steel material properties (isotropic, homogeneous with Young's modulus of 180GPa), bone material was given Young's modulus of 17GPa, assigned modulus of 0.1GPa for gap tissue material. In total four different FE models were created (Figure 18).
Principal strain components as well as the average principal strain and distortion were evaluated.

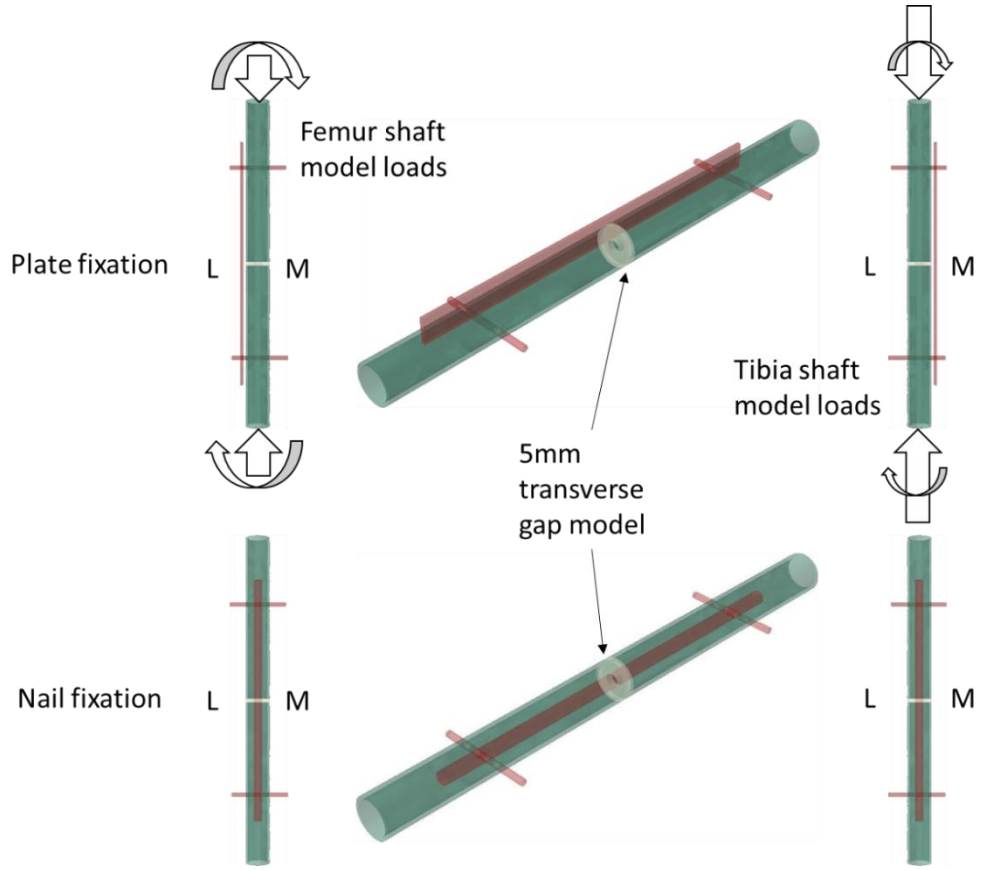

Figure 18: Idealized finite element models. Top: Plate fixation, for the femur (left), plate placed laterally (L); for the tibia (right), plate placed medially (M). Bottom: Nail fixation was symmetrical and thus there were no geometrical differences between femur and tibia models, but both models were loaded differently. A mid-shaft 5mm transverse fracture gap with regenerative tissue was modelled as well [11].

Simulation models were based on simultaneous contribution of all four loading scenarios: bone models were simultaneously tested with axial compression, medio-lateral and postero-anterior bending, and torsion (Table 14) (femur and tibia with its appropriate mechanical boundaries).

Loading	Femur	Tibia
Axial Compression	1500 N	3000 N
Medio-Lateral Bending	-75 Nm	-22.5 Nm
Postero-Anterior Bending	-18.75 Nm	112.5 Nm
Torsion	18.75 Nm	-22.5 Nm

Table 14: Bone-location matched loading for the femur and tibia according to the derived bone loads from Heyland et al. [23] for normal walking kinematics. Relative rehabilitation loads in patients are probably smaller due to reduced gait speed and the use of walking aids. Body weight exploited circa 75kg for all cases.

4.1.4 Statistical analysis

Statistical analyses were performed to evaluate possible significant differences of the study. ANOVA tests were performed to compare the different timepoints and cortical sides. Since not all groups related to cortex side showed normal distribution, post hoc

Mann-Whitney U tests were performed to highlight any difference (significant threshold at 5%). The same methodology was applied to study only femur and only tibia groups and tibia fixation treatments (nail/plate/combined treatment (nail + fibula plate)).

Regarding FE simulation, mean values of callus size and density for the subgroups of tibia/femur and plate/nail for the different localizations were compared with a linear regression, matching simulation results of strains (weighted for the number of cases in the clinical population).

4.2 Results

4.2.1 Femur

54 patients out of 63 femur cases had imaging at the given timepoints. 38 patients showed medial callus, 32 lateral, 32 ventral and 31 dorsal. Illustration of callus sizes and density as well as fracture healing in femur (mRUST) are shown in figures 19, 20 and 21.

Mean maximum relative callus size (regardless of the timepoints) was 0.82 cm2/cm (SD 0.44) for medial, 0.86 cm2/cm (SD 0.17) for lateral, 0.55 cm2/cm (SD 0.20) for ventral and 1.02 cm2/cm (SD 0.35) for dorsal callus.

At T1, highest mean size was dorsally (0.73 cm2/cm), followed by medial (0.69 cm2/cm), lateral (0.61 cm2/cm) and ventral (0.49 cm2/cm) (p=0.16). Overall highest callus size was found in T2 with dorsal size of 1.41 cm2/cm, medial of 1.18 cm2/cm, lateral of 0.96 cm2/cm and ventral one of 0.73 cm2/cm. At T3, callus size decreased for all sides except for lateral one, which slightly increased (dorsally (0.93 cm2/cm), medially (1.15 cm2/cm), ventrally (0.67 cm2/cm), laterally (0.98 cm2/cm)). Further size decreasing was observed at T4 medially (0.26 cm2/cm), laterally (0.9 cm2/cm) and ventrally (0.29 cm2/cm), while no callus was observed dorsally. Only one patient showed callus at this time point (Table 15).

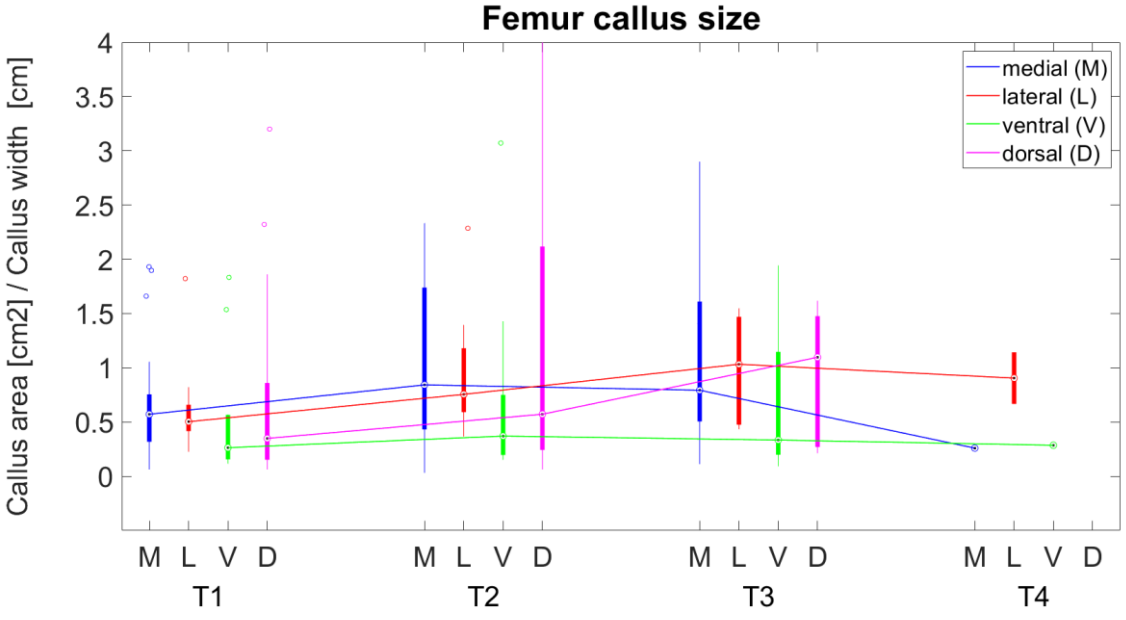

Figure 19: boxplots for callus size development on the femur population on the four cortices during the defined timepoints.

Femur callus size	Medial	Lateral	Ventral	Dorsal
T1	0.69±0.57	0.61±0.42	0.49±0.53	0.73±0.93
T2	1.18±1.11	0.96±0.62	0.73±0.91	1.41±1.57
T3	1.15±0.94	0.98±0.5	0.67±0.68	0.93±0.65
T4	0.26*	0.9±0.34	0.29*	/

Table 15: femur callus size results on the four cortices: values highlighted with the asterisk consist in single samples (only one value was available in the medial and ventral cortices on the last timepoint, while a complete lack was present dorsally).

Callus density (relative to cortical bone density) increased steadily from T1 (medial 0.86, lateral 0.88, ventral 0.9, dorsal 0.84) to T2 (medial 0.9, lateral 0.88, ventral 0.96, dorsal 0.87) in all regions. Callus density exceeded cortical density on ventral and dorsal portions (both 1.02), but not medially (0.9) and laterally (0.95) at T3. Further increments were found in T4 (medial 1.14, lateral 1.28, ventral 1.18), no callus was observed dorsally and only one patient showed callus medially and ventrally at this time point (Table 16).

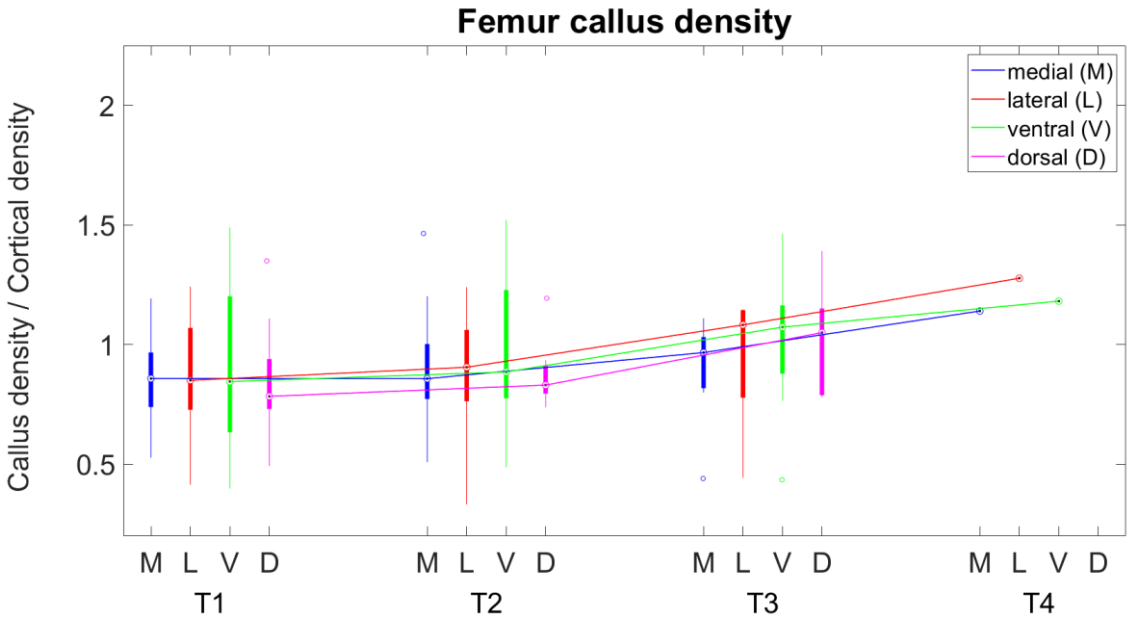

Figure 20: boxplots for callus density development on the femur population on the four cortices during the defined timepoints.

Femur callus density	Medial	Lateral	Ventral	Dorsal
T1	0.86±0.16	0.88±0.25	0.9±0.32	0.84±0.2
T2	0.9±0.22	0.88±0.28	0.96±0.3	0.87±0.13
T3	0.9±0.21	0.95±0.28	1.02±0.31	1.02±0.25
T4	1.14*	1.28±0.02	1.18*	/

Table 16: femur callus density results on the four cortices: values highlighted with the asterisk consist in single samples (only one value was available in the medial and ventral cortices on the last timepoint, while a complete lack was present dorsally).

Statistically significant differences were found with respect to lateral density with t-test comparisons, from T1 to T4 (p=0.022) and T2 to T4 (p=0.044), with higher value at last time-point.

mRUST scores increased from T1 (6.72) to T2 (9.62) and decreased slightly at T3 (9.5). Further increase was found in T4 (12.67) (Table 17).

	mRUST femur
T1	6.72±2.53
T2	9.62±3.5
T3	9.5±3.49
T4	12.67±3.21

Table 17: mRUST scores during the different timepoints at femur level.

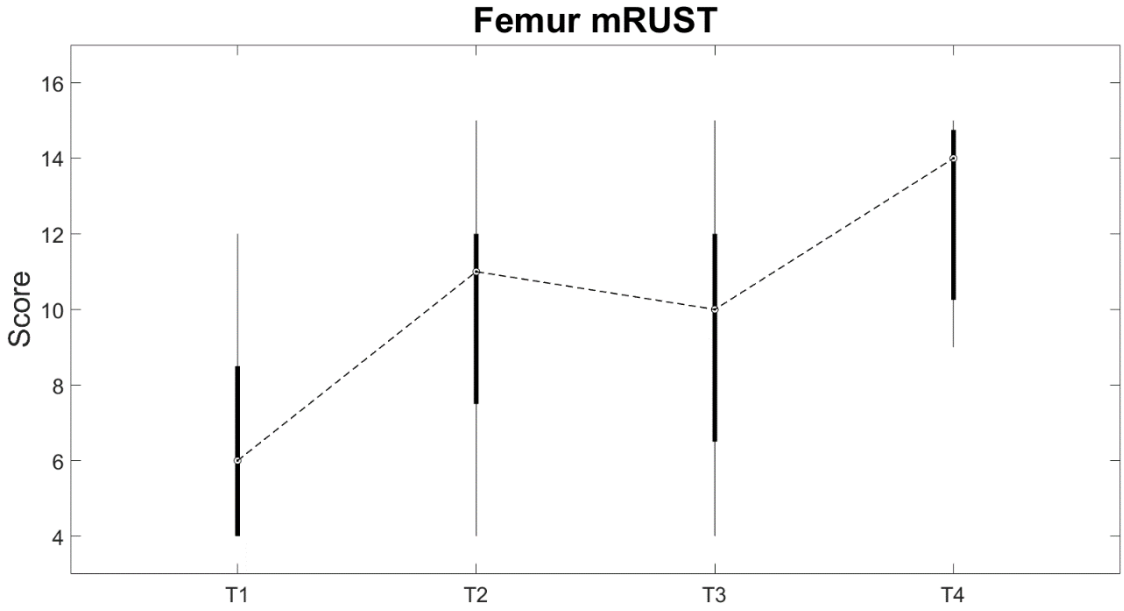

Figure 21: boxplots for trend of mRUST scores on femur fracture cases during follow-up stages, it's visible how the values increase rapidly from T1 to T2 and T3 to T4, a slowdown is highlighted from T2 to T3.

4.2.2 Tibia

63 patients of 103 tibia cases were identified with imaging at the given timepoints. 43 calluses medially, 37 laterally, 30 ventrally and 32 dorsally. Illustration of callus sizes and density as well as progress of fracture healing in tibia (mRUST) are shown in figures 22, 23 and 24.

Mean maximum relative callus size was 0.37 cm2/cm (SD 0.1) medially, 0.51 cm2/cm (SD 0.18) laterally, 0.29 cm2/cm (SD 0.1) ventrally and 0.38 cm2/cm (SD 0.09) dorsally.

For T1 highest mean callus size was found laterally (0.39 cm2/cm), followed by medial (0.31 cm2/cm), dorsal (0.3 cm2/cm) and ventral (0.19 cm2/cm) calluses (p=0.015). Overall highest callus size was measured at T2 with lateral callus size of 0.53 cm2/cm, dorsal of 0.47 cm2/cm, medial of 0.45 cm2/cm and ventral one by 0.31 cm2/cm. At T3, callus size kept increasing laterally (0.75 cm2/cm), medially (0.46 cm2/cm) and ventrally (0.43 cm2/cm), while a slight decrease was found dorsally (0.44 cm2/cm) (p=0.013).
At T4 all sides showed a decrease: medially (0.26 cm2/cm), laterally (0.36 cm2/cm), ventrally (0.24 cm2/cm) and dorsally (0.29 cm2/cm). Highest decrease was noted on the lateral side with an overall decrease of 48%.
Lateral and ventral groups were statistically different with respect to the time points, proving a significant change in size during the healing process, post hoc analyses showed significant difference on the medial portion from T1 to T2 (p=0.047) and T1 to T3 (p=0.041), lateral from T1 to T2 (p=0.039), T1 to T3 (p<0.01) and T2 to T3 (p=0.07) and ventral from T1 to T3 (p<0.01) and T2 to T3 (p=0.024). Furthermore, t-test comparisons with respect to the time point between callus sides proved differences between medial to ventral (p=0.05) and lateral to ventral (p<0.01) at T1 and same trend in T2 (medial vs ventral (p=0.035), lateral vs ventral (p<0.01)) (Table 18).

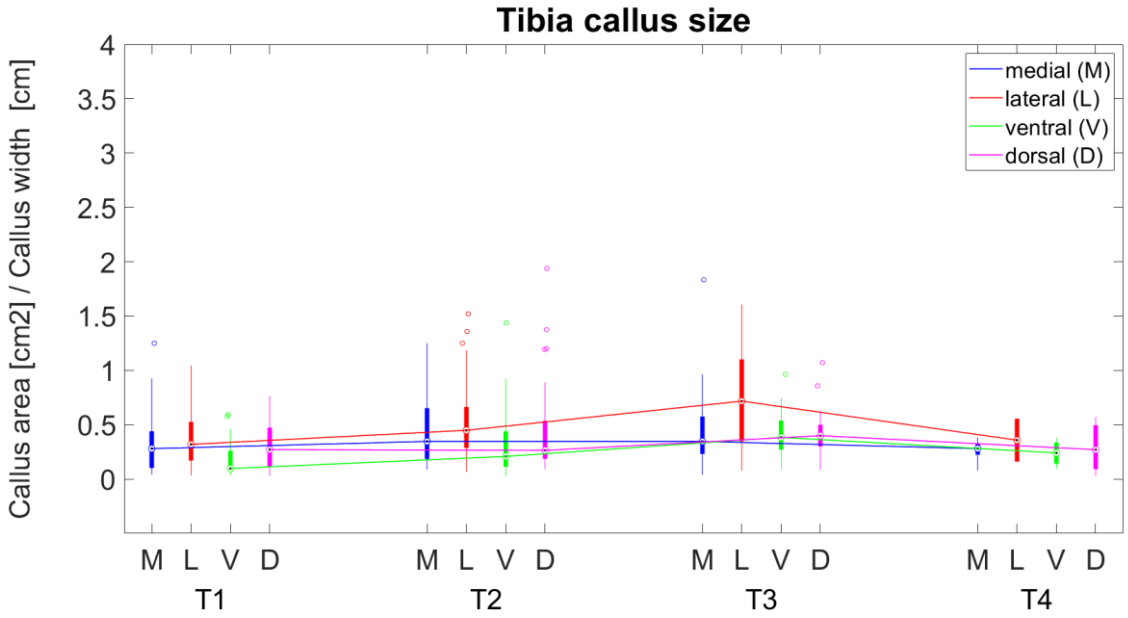

Figure 22: boxplots for callus size development on the tibia population on the four cortices during the defined timepoints.

Tibia callus size	Medial	Lateral	Ventral	Dorsal
T1	0.31±0.28	0.39±0.27	0.19±0.17	0.3±0.22
T2	0.45±0.34	0.53±0.35	0.31±0.3	0.47±0.46
T3	0.46±0.36	0.75±0.49	0.43±0.22	0.44±0.24
T4	0.26±0.11	0.36±0.28	0.24±0.13	0.29±0.27

Table 18: tibia callus size results on the four cortices.

Callus density increased steadily from T1 (medial 0.75, lateral 0.8, ventral 0.98) to T2 (medial 0.88, lateral 0.83, dorsal 0.87) for all regions except ventrally (slight decrease from 0.98 to 0.97). In T3 all densities decreased with respect to T2 except for the lateral region (same value of T2), with values of 0.84, 0.83, 0.82 and 0.94 (respectively for medial, lateral, ventral and dorsal side). In the last time point a lack of data for ventral and dorsal callus was present, so only a further decrease of medial (0.68) and increase of lateral one (0.92) could be noted (Table 19).

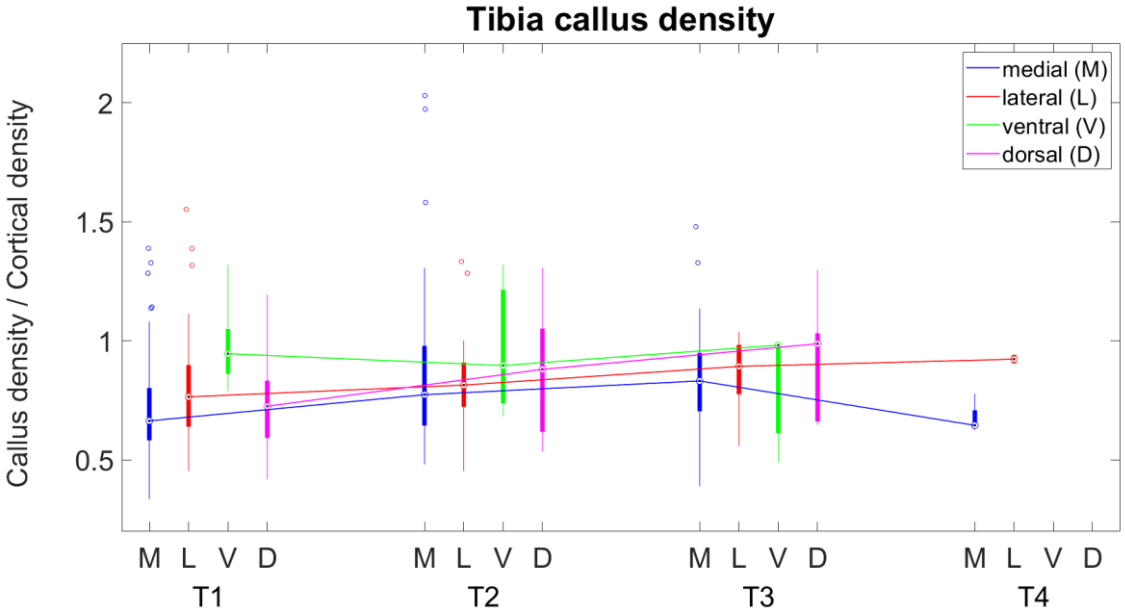

Figure 23: boxplots for callus density development on the tibia population on the four cortices during the defined timepoints.

Tibia callus density	Medial	Lateral	Ventral	Dorsal
T1	0.75±0.28	0.8±0.23	0.98±0.2	0.74±0.2
T2	0.88±0.37	0.83±0.16	0.97±0.32	0.87±0.28
T3	0.84±0.23	0.83±0.22	0.82±0.29	0.94±0.25
T4	0.68±0.06	0.92±0.03	/	/

Table 19: tibia callus density results on the four cortices (lack of data was present on the ventral and dorsal cortices in T4).

No significant differences were found with ANOVA tests, while post hoc analyses proved significant variations between medial density from T1 to T3 ($p=0.042$) and T3 to T4 ($p=0.032$) and, at T1, between medial and ventral ($p=0.029$), lateral to ventral ($p=0.046$) and ventral to dorsal ($p=0.019$).

mRUST scores increased constantly over the timepoints from T1 (7.42), T2 (10.37), T3 (12.96), to T4 (14.22) (Table 20).

	mRUST tibia
T1	7.42±2.2
T2	10.37±2.88
T3	12.96±2.97
T4	14.22±1.86

Table 20: mRUST scores during the different timepoints at tibia level.

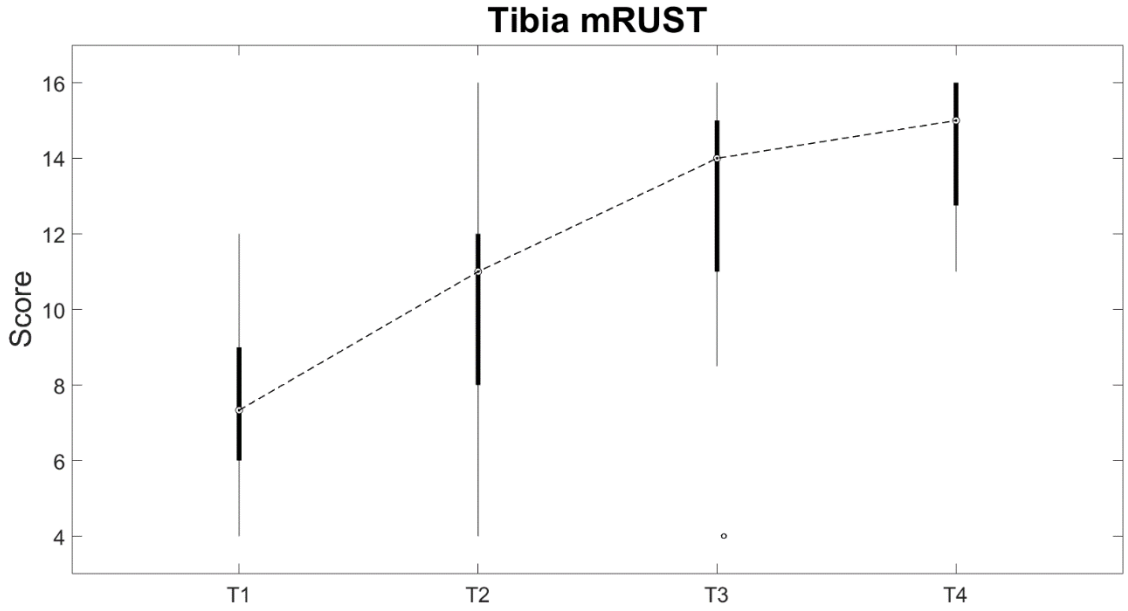

Figure 24: boxplots for trend of mRUST scores on tibia fracture cases during follow-up stages, it's visible how the values increase rapidly constantly from T1 to T3, with a slight decrease from T3 to T4.

4.2.3 Comparison between femur and tibia

Callus sizes in the femurs were overall larger compared to callus sizes in tibia with mean differences of 0.45 cm2/cm medially, 0.36 cm2/cm laterally, 0.25 cm2/cm ventrally and 0.65 cm2/cm dorsally. Highest differences between total callus sizes were observed at T2 (2.52 cm2/cm), followed by T3 (1.66 cm2/cm) and T1 (1.33 cm2/cm), while differences at T4 were lower (0.3 cm2/cm). Medial callus size differed statistically in T1 and T2 between femur and tibia, respectively with p=0.014 and p=0.02.

Mean callus density was slightly higher for all regions in femur with a mean difference of 0.16 cm2/cm medially, 0.15 cm2/cm laterally, 0.09 cm2/cm ventrally and 0.06 cm2/cm dorsally. Mean overall density of the callus in femur and tibia differs by 0.45 at T1, 0.36 at T2, 0.25 at T3 and 0.65 at T4, however only a few data points were available at the last time point T4. Callus density exceeded cortical density (density > 1) in femur at T3 ventrally and dorsally and at T4 medially and laterally, same phenomenon wasn't found in tibias (max: 0.97 cm2/cm ventrally at T3). Femur density showed an approximately continuous rise, while for the tibia, only small changes during follow-up were registered,

with overall slight increasing from T1 to T2 (except for ventral side). No statistical differences were found on callus densities between femur and tibia populations.

mRUST showed higher values in tibia at all timepoints with differences of 0.5 at T1, 0.75 at T2, 3.46 at T3 and 1.55 at T4, however only at T3 significant statistical differences were found ($p<0.01$). Healing rate was higher in tibia with respect to femur (Figures below).

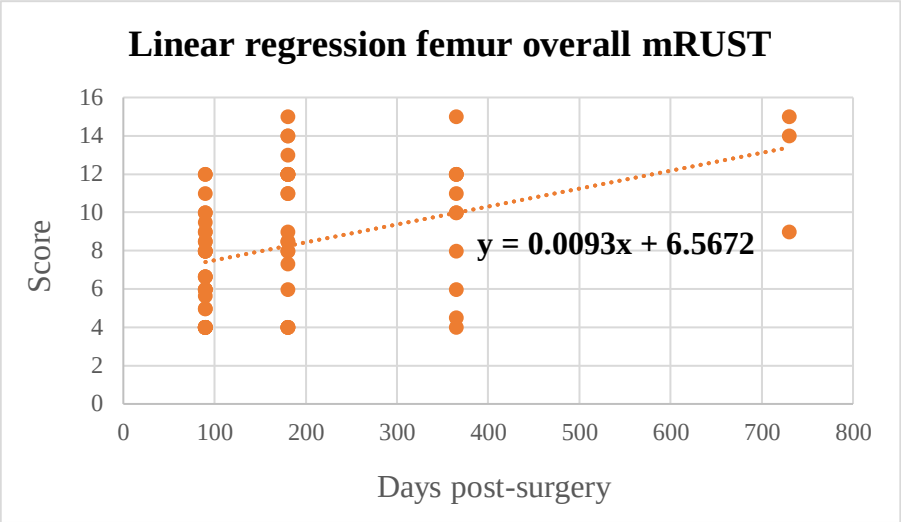

Figure 25: Linear regression ($p<0.01$) with respect to mRUST femur scores at four defined follow-up stages: T1: 90 (± 45d) days post-surgery, T2: 180 (± 45d) days post-surgery, T3: 365 (± 45d) post-surgery, T4: 730 (± 45d) days post-surgery).

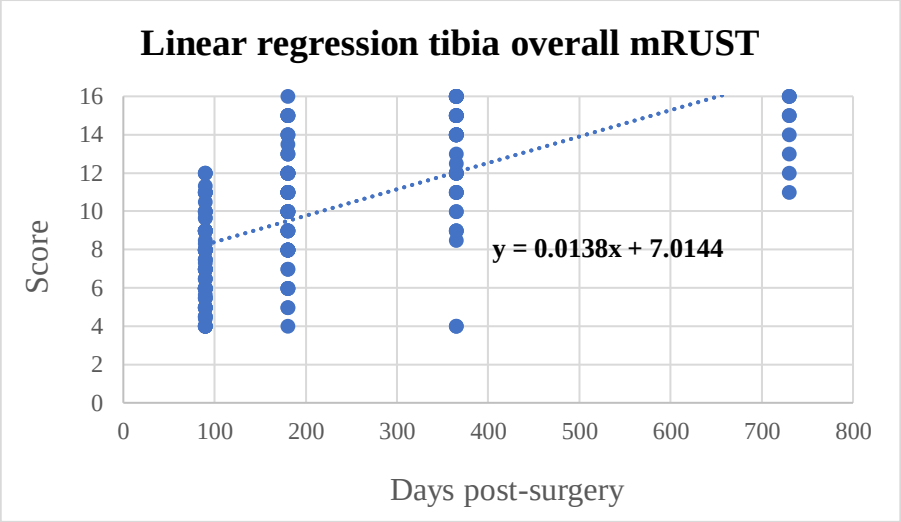

Figure 26: Linear regression ($p<0.01$) with respect to mRUST tibia scores at four defined follow-up stages: T1: 90 (± 45d) days post-surgery, T2: 180 (± 45d) days post-surgery, T3: 365 (± 45d) post-surgery, T4: 730 (± 45d) days post-surgery).

As it could be highlighted, different value of regression was found on tibia population (0.0138), with respect to femur (0.0093), with an overall mRUST tibia score increase over time 48.39 % higher than femur.

4.2.4 Fixation treatment

Limited data were present to assess callus characteristics according to fixation in femur fractures, so, only tibia cases were considered for further studies. Illustration of callus sizes and progress of fracture healing for different fixation treatments (mRUST) are shown in figures 27, 28, 29 and 30.
Plate treatment showed an overall increase on all regions from T1 to T3, with highest values reached laterally (1.3 cm2/cm) and ventrally (0.54 cm2/cm), with respect to medial (0.21 cm2/cm) and dorsal (0.46 cm2/cm) portions.
ANOVA tests highlighted differences in lateral callus with respect to the time points ($p<0.01$) and in T3 between regions ($p=0.015$). Furthermore, post hoc analyses showed significant variations between lateral and ventral calluses in T1 and T2 ($p<0.01$ in both) and between lateral and dorsal ones in T3 ($p=0.03$) (Table 21).

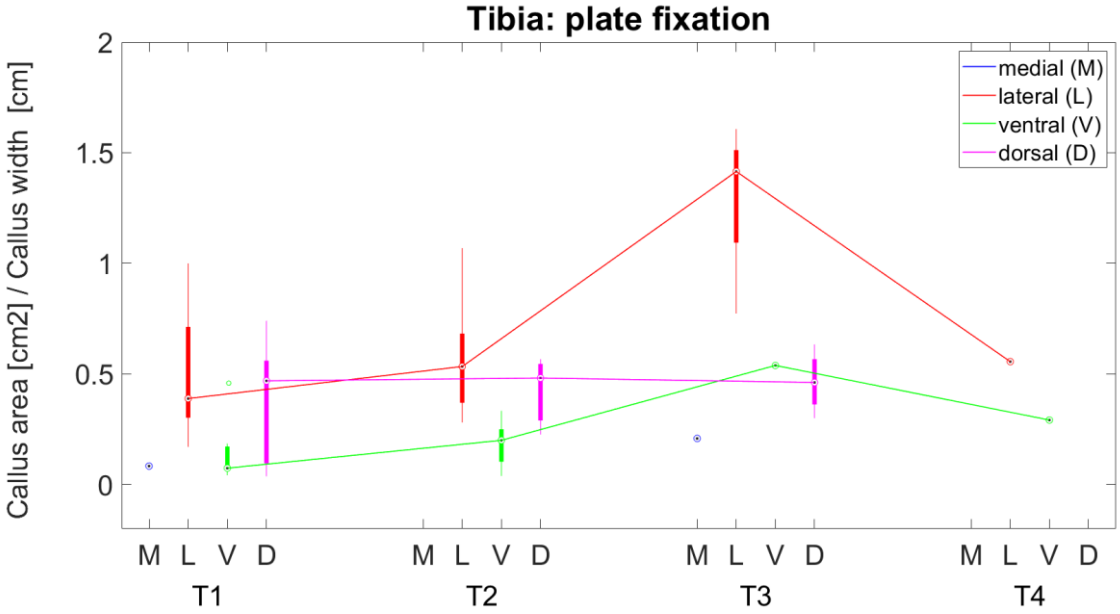

Figure 27: boxplots for callus size development on the tibia population with plate fixation on the four cortices during the defined timepoints.

Tibia callus size (plate)	Medial	Lateral	Ventral	Dorsal
T1	0.08*	0.5±0.29	0.15±0.14	0.37±0.29
T2	/	0.57±0.25	0.18±0.11	0.42±0.18
T3	0.21*	1.3±0.36	0.54*	0.46±0.14
T4	/	0.56*	0.29*	/

Table 21: tibia callus size with plate treatment on the four cortices: values highlighted with the asterisk consist in single samples (only one value was available in the medial cortex in T1 and T2, lack in T3 and T4, singular value laterally in T4. Ventrally singularities in T3 and T4 while dorsally lack in T4).

In the nail case, only the lateral callus kept increasing for the entire follow-up stage, reaching the highest value registered at 0.54 cm2/cm, while the other regions increased only from T1 to T2 and then started decreasing until T4, with values approximately similar between medial, ventral and dorsal portions. No statistical differences were found, proving an overall homogeneous development of callus in all regions (Table 22).

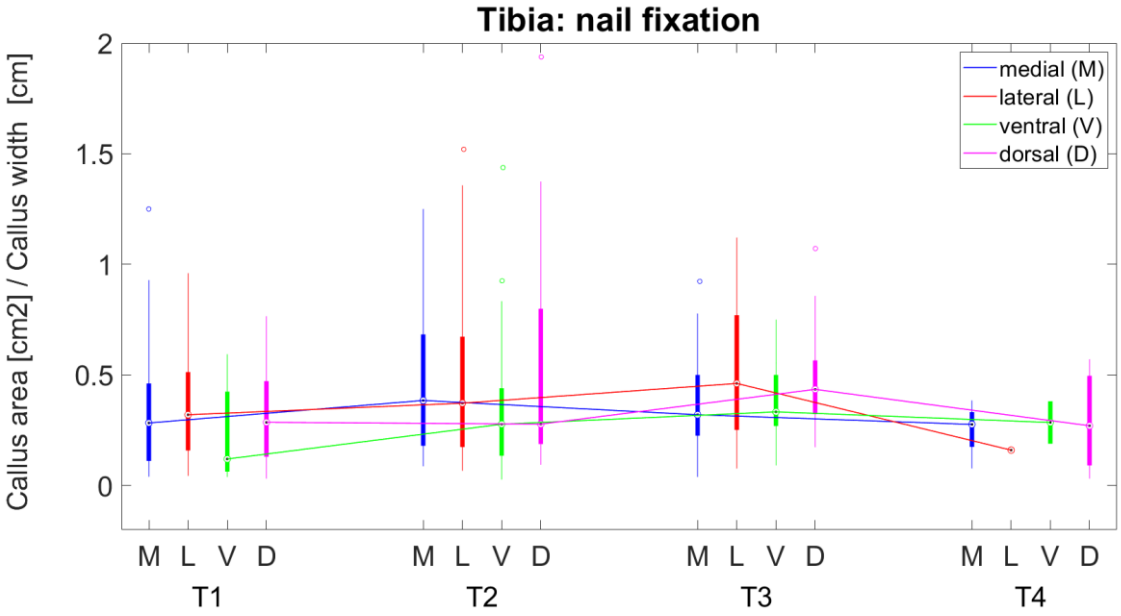

Figure 28: boxplots for callus size development on the tibia population with nail fixation on the four cortices during the defined timepoints.

Tibia callus size (nail)	Medial	Lateral	Ventral	Dorsal
T1	0.33±0.31	0.25±0.13	0.23±0.21	0.32±0.22
T2	0.48±0.35	0.37±0.27	0.39±0.36	0.52±0.51
T3	0.37±0.21	0.51±0.41	0.37±0.19	0.49±0.29
T4	0.25±0.13	0.54±0.37	0.29±0.14	0.29±0.27

Table 22: tibia callus size with nail treatment on the four cortices.

The combination of nail and fibular plate favoured a constant increase in callus size for all regions from T1 to T3, not present in nail alone, reaching maximum values of 0.73 cm2/cm, 0.71 cm2/cm, 0.49 cm2/cm and 0.31 cm2/cm (respectively for medial, lateral, ventral and dorsal). In T4 data from one patient were available, showing radical decrease in medial and ventral regions (Table 23).

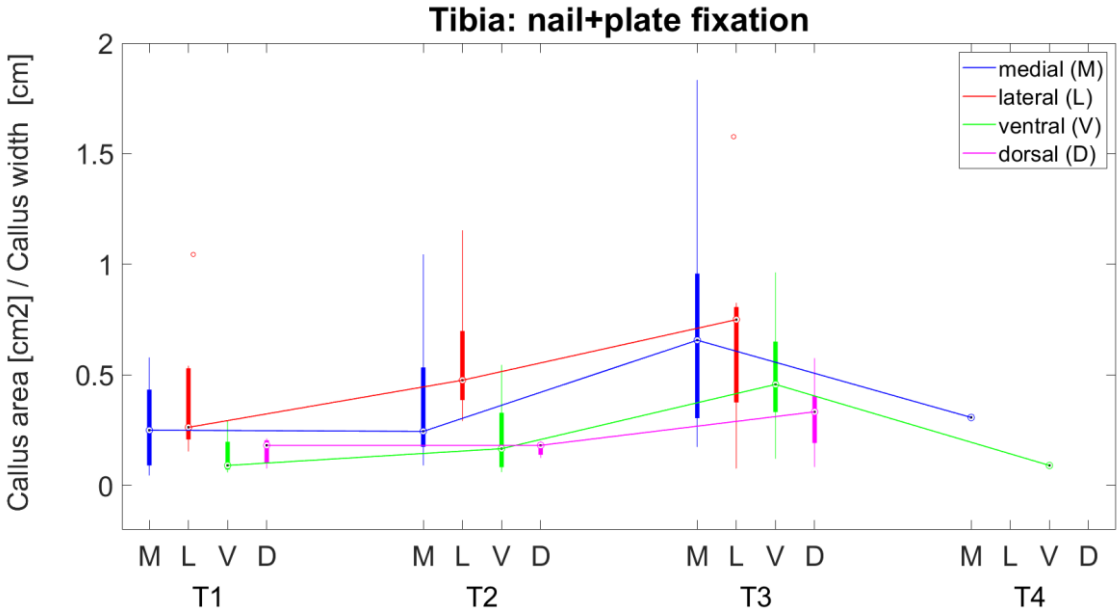

Figure 29: boxplots for callus size development on the tibia population with nail+plate fixation on the four cortices during the defined timepoints.

Tibia callus size (nail+plate)	Medial	Lateral	Ventral	Dorsal
T1	0.27±0.2	0.39±0.28	0.14±0.1	0.16±0.07
T2	0.38±0.32	0.56±0.28	0.23±0.19	0.17±0.04
T3	0.73±0.55	0.71±0.48	0.49±0.27	0.31±0.18
T4	0.31*	/	0.09*	/

Table 23: tibia callus size with plate treatment on the four cortices: values highlighted with the asterisk consist in single samples (only one value was available in the medial cortex in T4, lack laterally in T4, singular value ventrally in T4 and again lack in T4 dorsally).

Cross-comparison between fixation treatments showed only a relevant difference of lateral callus between nail and plate in T3 ($p=0.011$), with a larger callus with plate treatment.

Finally, mRUST scores highlighted higher values for both combination treatment and nail with respect to plate, with an approximately constant increase in score present only in the combined treatment (highest value at 16), while plate and nail showed a slightly minor trend from T3 to T4 (reaching respectively 11 and 14.43). Statistical differences were found only between plate and nail scores in T1 and T2 (respectively $p=0.041$ and $p<0.01$) (Table 24).

mRUST tibia fixation

	Plate	Nail	Nail+Plate
T1	6.54±2.08	7.74±2.15	7.57±2.38
T2	8.42±2.57	10.99±2.77	10.64±2.87
T3	10.39±4.33	13.72±2	13.2±2.74
T4	11*	14.43±1.51	16*

Table 24: mRUST scores during the different timepoints at tibia level for plate, nail, and nail+fibular plate fixation treatments, values highlighted with the asterisk consist in single samples.

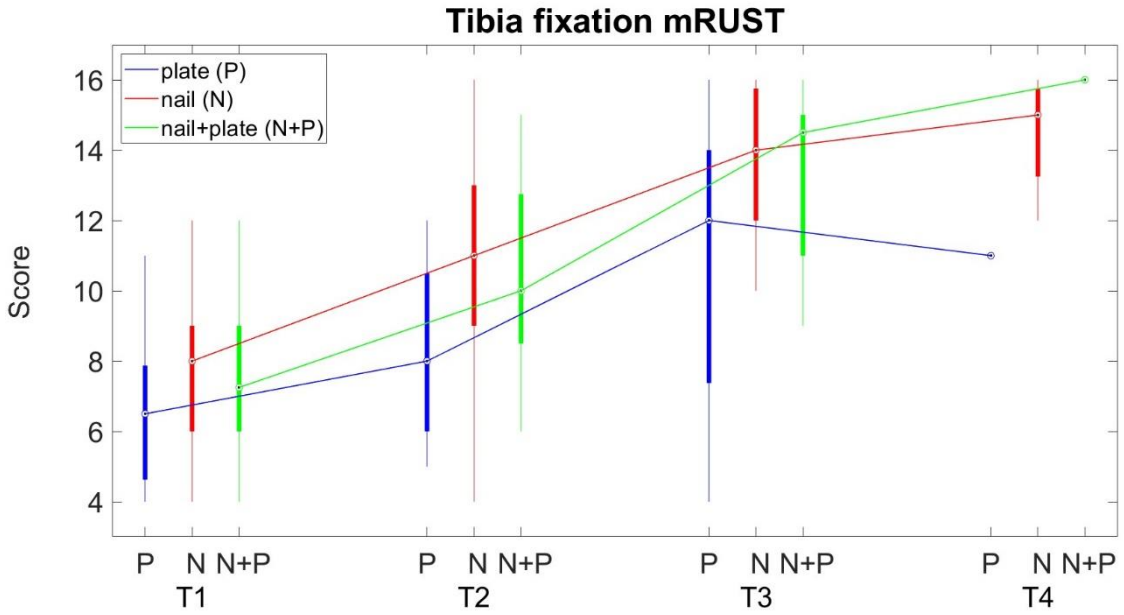

Figure 30: boxplots for mRUST score for tibia cases with intramedullary nail, plate and nail+fibular plate treatments. Overall nail and nail+plate reach higher scores in a faster and more regular trend.

Tibia fractures treated with plates produced bigger calluses with respect to the nail, with maximum values at T3 for plate cases and T2 for nails. No specific differences were found between callus sides, except for the plate, where lateral callus was higher than medially.

4.2.5 Finite Element Analysis (FEA) strain component correlations with callus density and size

Strain components were influenced by location (bone type and relative location within it) and fixation (Fig. 31). An interaction between the relative position in the bone with the fixation type and bone loading was highlighted: the largest callus occurred dorso-medially in the femur, while plates were attached laterally in the femur; largest callus appeared laterally in the tibia, while plates were attached medially in the tibia shaft (Table below, Figure below). A similar trend was found for the intramedullary nailing, where highest strains occurred medially in the femur and dorso-laterally in the tibia, but overall strain (median of min./max. principal strain -3.8%, median of distortion -0.6%) appeared smaller for nailing compared to plating. Median strains in tibia gap tissue were higher for max. principal strain (+24.2%) and distortion (+10.6%) components, but slightly lower for min. principal strain (-2.8%) compared to femur.

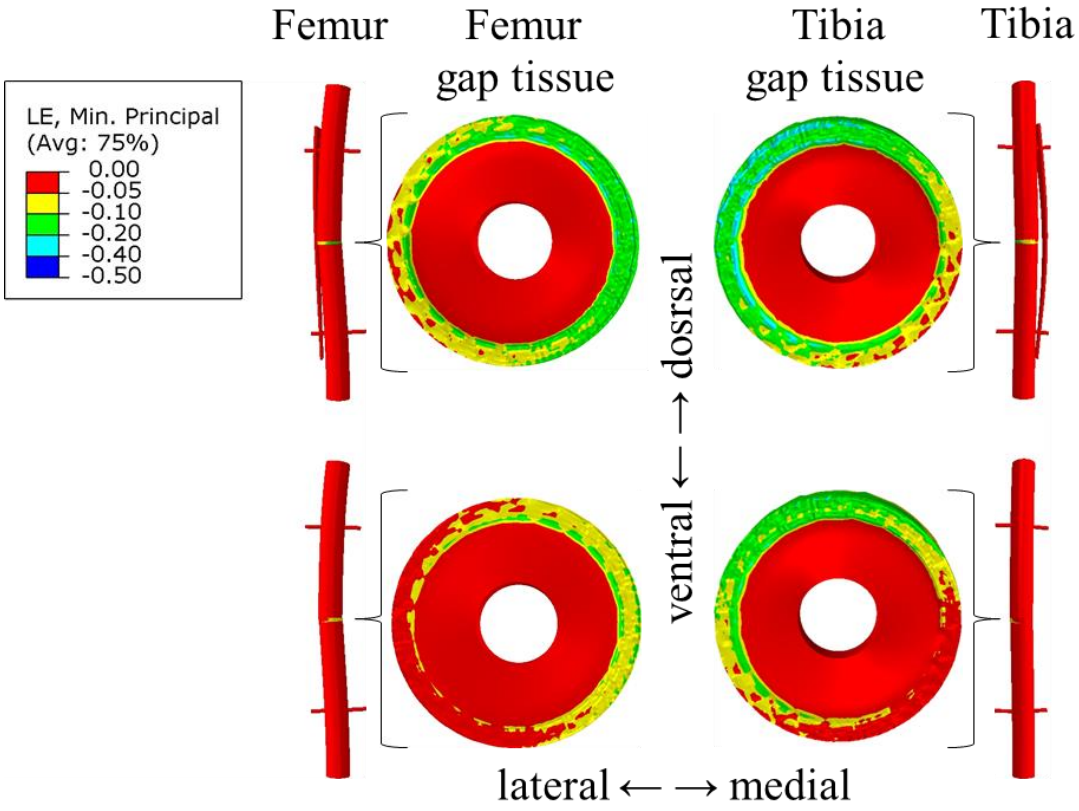

Figure 31: Finite element strain results of different fixation options (top: plating, bottom: nailing; 5x exaggerated deformation) and different bone loading scenarios (left: femur loading, right: tibia loading; respectively), centrally, the gap tissue minimum principal strain is shown with the dorsal aspect on top, ventral at the bottom, lateral aspect to the left and medial aspect to the right [11].

The best fit of a model correlation of strain components was achieved with callus density (Table 25), followed by callus density*size and the weakest correlation occurred with callus size. Distortion of gap tissue (shear, i.e. strain without volume change) was a consistently strong negative predicting correlation factor of callus density*size and especially callus density. Minimum principal strain was the strongest positive predictor of callus density, while max. principal strain was the strongest predictor of callus density and callus density*size.

Model factor (standardized influence)	Model callus density	Model callus size	Model callus density * size
Max. principal strain	**9.71**	0.49	**10.54**
Mid. principal strain	0	0	0
Min. principal strain	**3.54**	**1.62**	**1.6**
Dilatation (volume change)	-0.1	-0.05	-0.12
Distortion (Shear)	**-16.94**	**-4.1**	**-14.41**
Dilatation/Distortion	0	0.04	0
Constant	4.65	3.03	3.19

Table 25: Linear regression factor influences for the association of strain components to callus density, size and callus density*size.

4.3 Limitations and Discussion

Results showed how bone type and fixation system are associated to the callus development. Femur cases produced relatively denser and larger callus with respect to tibia. At the same time, healing process showed different trends: while tibia cases tended to constantly increase over timepoints, femoral fractures showed a slower callus development, reaching lower values on mRUST at the last follow-up stage.

Fixation analysis highlighted how the healing process can be influenced by the type of treatment. Plate cases produced larger callus with respect to the others, but less homogenous. Nails and composition of nail+plate granted higher stability of the fracture, permitting a more homogenous load's transmission and more uniform interfragmentary movement. In this way the callus developed may could reach lower size values, due to the accentuated stability, but cortices with similar values. Plates instead, being fixed on a specific side, granted higher stability on certain cortices and more freedom of movement on the others, producing more irregular bone calluses. Also, mRUST results proved how plate treatments reached lower values with respect to the others that were able to attain optimal values from 14 to 16.

Notable differences in the strain components according to location and fixation were found (Figure 31). The exact strain values strongly depended on assumed gap tissue properties (gap size and stiffness). However, it wasn't generally true that strains onto the gap tissue were beneficial for larger callus density and size (max. or min. principal strain), while shear strain (distortion) was consistently detrimental and associated with smaller and less dense callus.

At the same time, strains were slightly lower with nail fixation, but higher for max. principal strain and distortion in the tibia. The higher distortion in tibia (approx. 10%) might explain the smaller and less dense callus, but it isn't clear why tibia healing rate remained higher than femur. Furthermore, rising callus size and the compensating effect of callus on lower tissue strain weren't considered in simulations. Also, the used implants and loads were idealized, and their effects might differ in situ.

The lack of available data also caused an approximated analysis of callus development in the majority of final timepoints for all samples (except for tibia callus size and tibia treated with nails).

5. ANALYSIS OF JOINT LOADING RELATIONSHIP WITH MULTIPLE PHYSIOLOGICAL FACTORS

Mechanical factors play a fundamental role in tissue regeneration, particularly in the bone tissue, where early healing phases can be disrupted by mechanical overloading. As previously seen in the introduction, patient-specific factors can influence the outcome of fracture healing. Loading is a key factor, which aligns with the "diamond concept": emphasizing osteogenic cells, osteoinductive mediators, osteoconductive matrix, and mechanical loading stability [18, 40].

Despite the importance of mechanical conditions, few studies have quantified them at fracture locations and so, biomechanical data have been rarely collected from fracture patients during rehabilitation stages. Exploiting data from previous studies [23], the aim was to estimate the load of fracture patients based on their characteristics such as patient weight and height, varus-valgus leg alignment and variables' combination, with a simple regression model. Consequently, it could be possible to estimate an association between local loading and healing outcome.

5.1 Materials and Methods

5.1.1 CAMS-Knee database

The Laboratory for Movement Biomechanics at ETH Zurich developed a single plane moving fluoroscope able to track human joints throughout complete cycles of daily activities to accurately reconstruct 3D joint kinematics, such as the knee joint, without soft tissue artefacts. Combined to this, telemetric implants developed at Charité Universitätsmedizin Berlin allowed a deeper understanding of internal loading conditions in subjects with embedded artificial joints. These implants are based on strain gauges fixed within the tibial component, able to capture tibio-femoral forces and moments during dynamic activities in human knee joints in vivo [45].

(CAMS-Knee) is a robust and meticulously curated collection of data designed for in-depth analysis and evaluation of knee-related musculoskeletal conditions, including radiographic images, medical and surgical records, clinical assessments and patient-reported outcomes [52].

5.1.2 Musculoskeletal modelling

The musculoskeletal model (Fig. 32). was based on the 3D patient specific anatomy reconstructed from ground reaction forces, CT images and kinematic input from gait analysis [46, 47], to allow estimation of muscle forces and joint loads for the whole leg. The musculoskeletal analysis exploited was based on the CAMS-Knee Dataset and was performed for each patient to estimate the muscle and joint contact forces in the lower limb as described previously [47]. More specifically: the lower limb kinematics were obtained from motion of markers on the skin [46] and combined with the functional flexion knee axis derived from the fluoroscopic TF kinematics [20, 45], as input for an

inverse dynamics approach. The subsequent muscle optimisation was based on minimising the sum of muscle stresses squared but was constrained to match the magnitude of the TF contact force measured in vivo to within 5%.

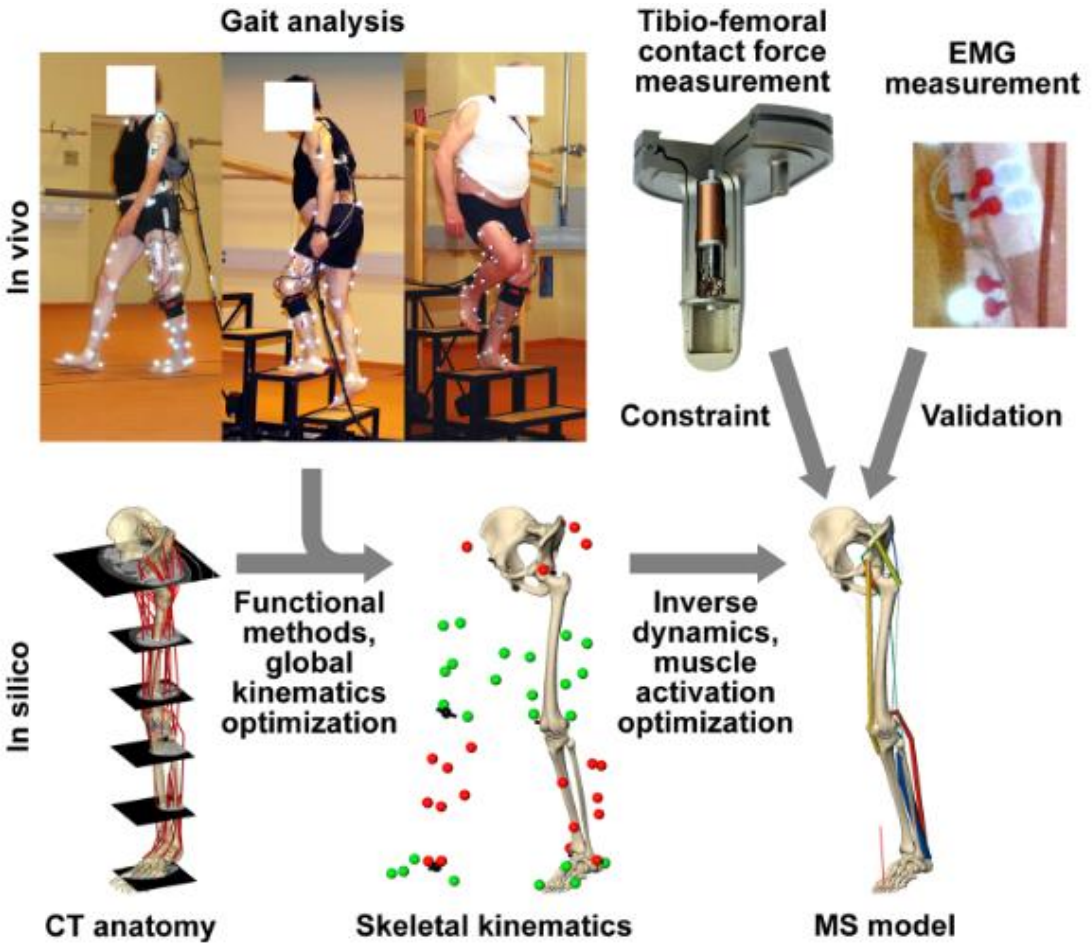

Figure 32: Overview of the steps to assess internal loading. Gait analyses were performed during walking and stair negotiation, with simultaneous measurement of the in vivo tibio-femoral forces and surface EMG of the main muscles. CT from patient skeletal anatomy was used to adapt reference muscles geometries, and then combined with determined joint centres/axes to obtain the skeletal kinematics. The resulting musculoskeletal models were constrained to match in vivo forces and EMG measurements obtained [47].

5.1.3 Subjects

For this study, data were collected from six subjects, (Table 26) were collected from the database (5 M, 1 F, aged 68 ± 5 years, mass 88 ± 12 kg, height 173 ± 4 cm) each of them with an instrumented total knee replacement [19]. Measurements were performed 5-7 years post-surgery during repetitions of multiple exercises of activities of daily living (Table 27).

Subject	K1L	K2L	K3R	K5R	K7L	K8L
Gender	M	M	M	M	F	M
Age	69	78	77	66	79	70
Body Mass [kg]	101	91	100	96	67	79
Height [cm]	175	169	173	174	165	175
Time post-op [months]	87	84	76	69	67	64
Tibio-femoral angle [degree]	3,0 varus	5,0 varus	3,5 varus	1,0 varus	6,5 varus	4,0 varus
Posterior slope [degree]	5	11	10	7	7	11

Table 26: Subjects' characteristics [52].

Activity	Description
Level Walking	Walking straight ahead over 5 force plates embedded in the floor
Stair descent	Walking down an instrumented stair with three steps, each 18 cm in height
Sitting and raising from a chair	The two tasks stand-to-sit and sit-to-stand were measured as a single sequence. The subject started in a sitting position, rose to an upright standing position and sat down again

Table 27: Activities performed [52].

The implanted system allowed to measure all the six load components (Fig. 33). For the study, the focus was mainly on the maximum resultant force on the joint.

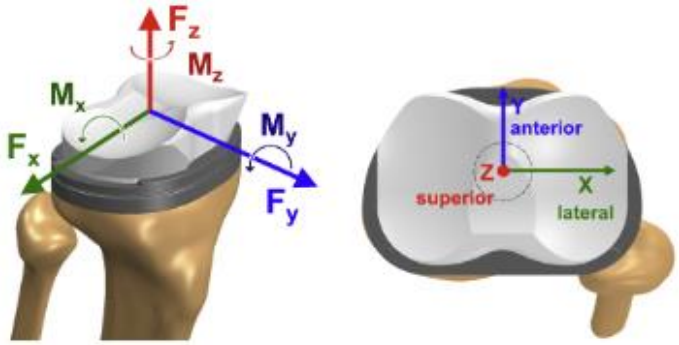

Figure 33: Coordinate system of the instrumented tibial tray [28].

5.2 Results

Data were collected and elaborated via a custom program in MatLab (MatLab R2022b, Matworks). Linear regression was calculated between the internal loads and body weight with respect to the task for the entire cohort, then the same process was repeated for load - varus angle relationship, load - (body weight*varus angle). Also, RMSE and r-squared were analysed (Table 28 and figures from 34 to 38).

Correlation Coefficient (r)			
Motor Task	**F - BW**	**F - varus**	**F - (BW*varus)**
Level Walking	0.62	0.36	0.72
Sit Down	0.73	0.81	0.84
Stairs Down	0.71	0.60	0.75
Stand Up	0.90	0.82	0.93
R-squared			
Level Walking	0.38	0.13	0.51
Sit Down	0.53	0.66	0.70
Stairs Down	0.51	0.36	0.57
Stand Up	0.80	0.68	0.86

Table 28: Correlation coefficients and determination coefficients for the different activities regarding the relationships between force - body weight, force - varus angle and force - composition body weight and varus angle.

Highest correlation between resultant force and body weight was found for the “Stand Up” activity at 0.90, lowest in “Level Walking” with 0.62. Similar trend was noted for force-varus angle correlation (highest “Stand Up” at 0.82, lowest at “Level Walking” 0.36) and force combined with product between body weight and varus angle (highest for “Stand Up” at 0.93, lowest in “Level Walking” 0.72), coefficients of determination followed the same trend.

Even though variables combination showed similar correlation trends, the results were different. Resultant joint force was less affected from varus angle rather than body weight, while the combination of weight and varus angle proved highest impact for all activities. This was furtherly proved by the correlation p-value, always lower than 0.001, confirming significant statistical correlation.

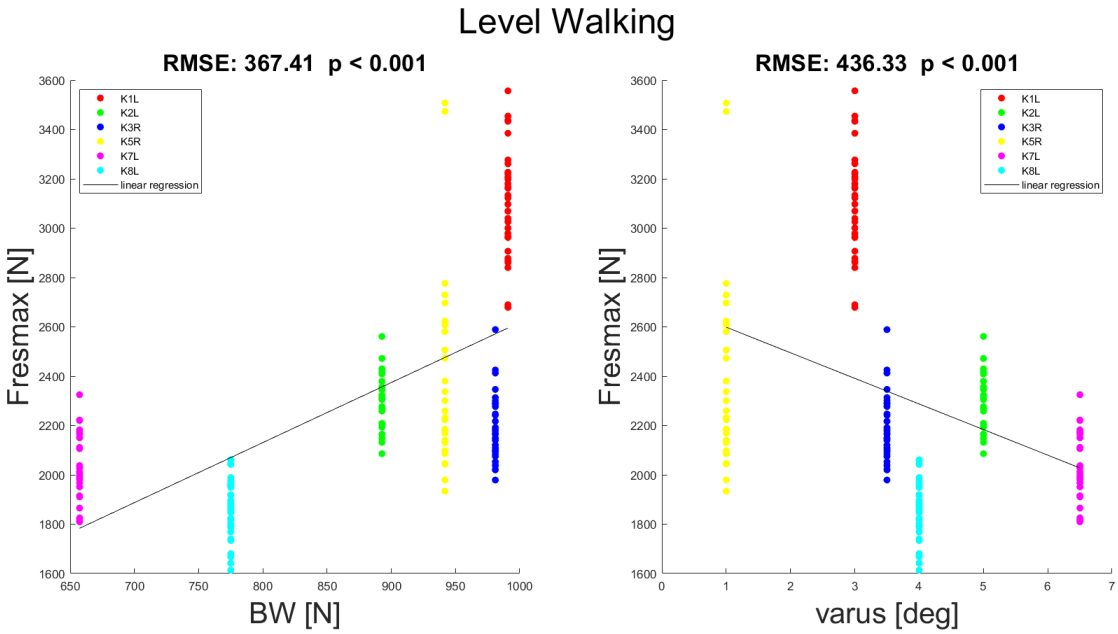

Figure 34: Linear correlation between maximal resultant force in the joint (registered by knee implant) and bodyweight (left) and varus angle (right) for “Level Walking” activity from the patients’ cohort.

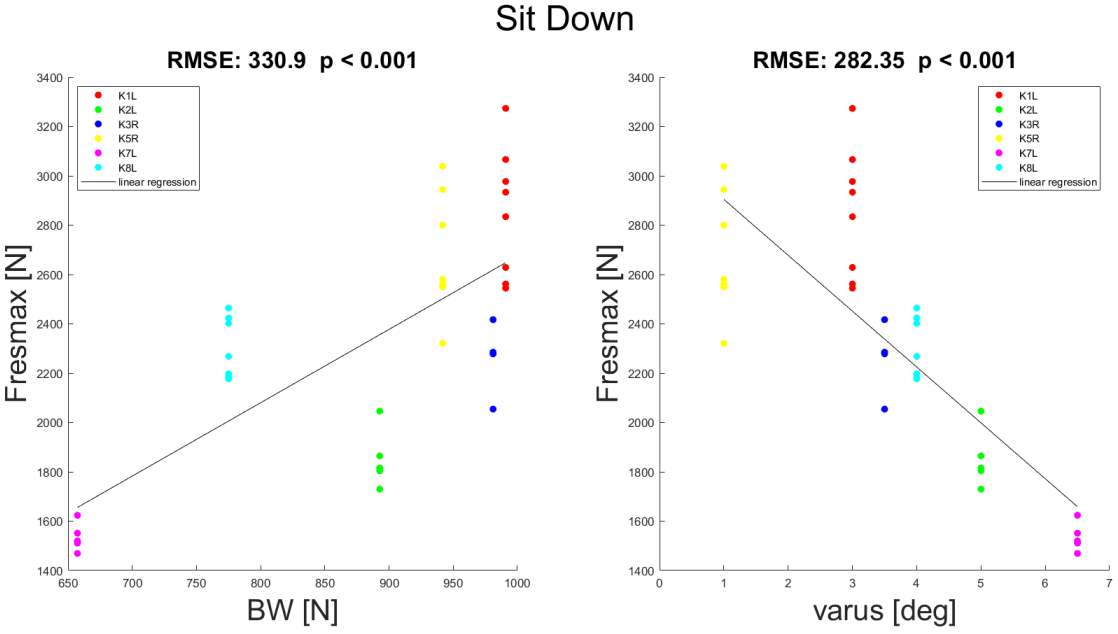

Figure 35: Linear correlation between maximal resultant force in the joint (registered by knee implant) and bodyweight (left) and varus angle (right) for “Sit Down” activity from the patients’ cohort.

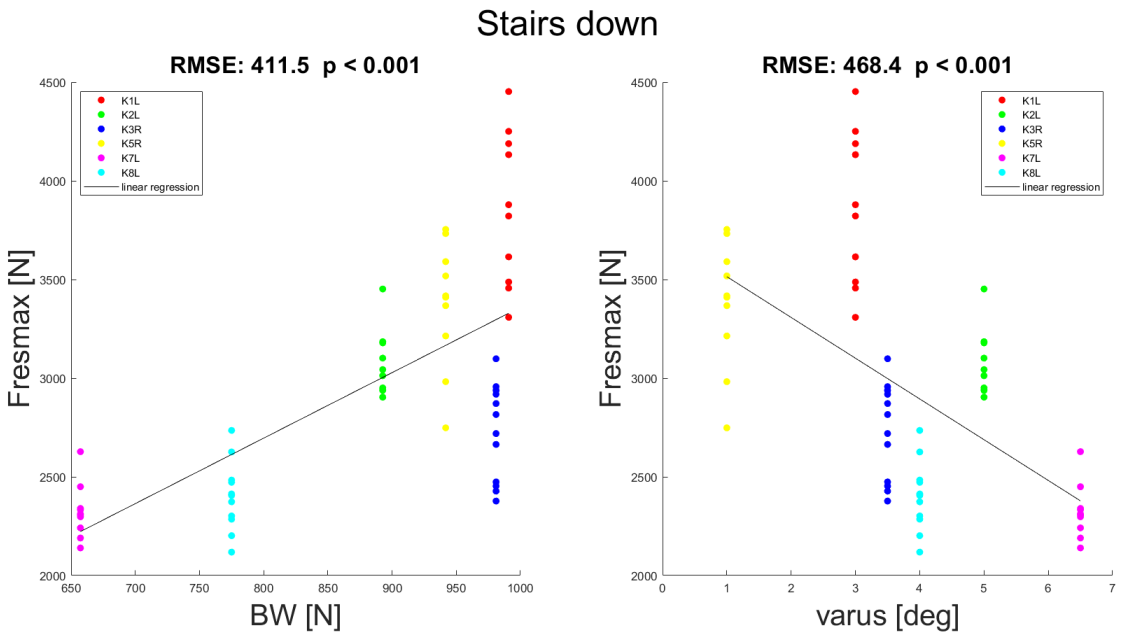

Figure 36: Linear correlation between maximal resultant force in the joint (registered by knee implant) and bodyweight (left) and varus angle (right) for "Stairs Down" activity from the patients' cohort.

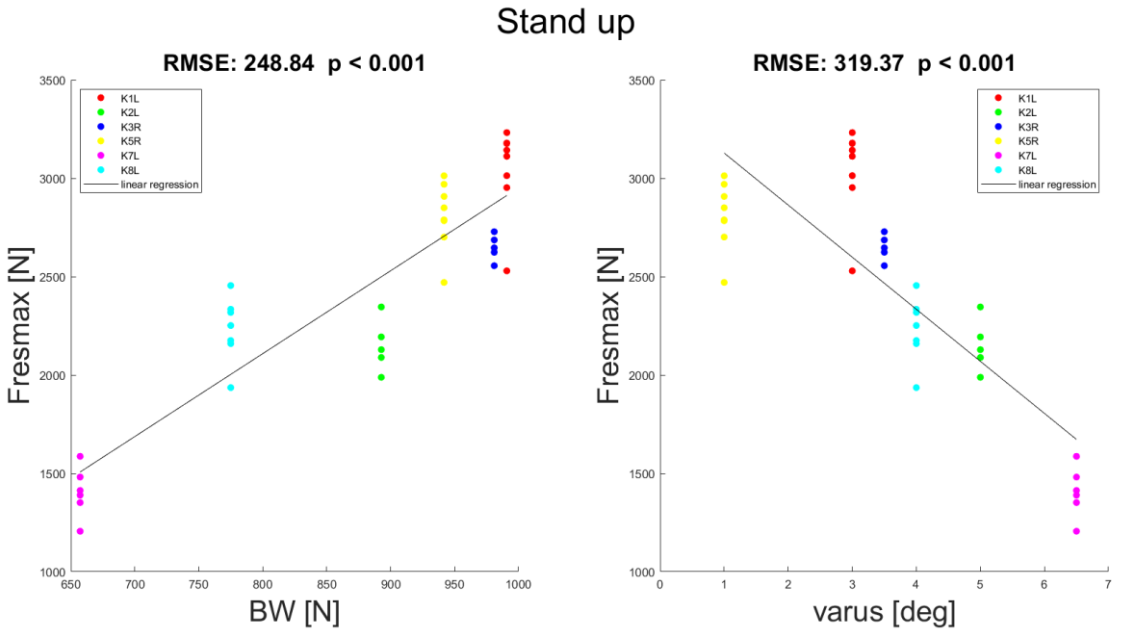

Figure 37: Linear correlation between maximal resultant force in the joint (registered by knee implant) and bodyweight (left) and varus angle (right) for "Stand Up" activity from the patients' cohort.

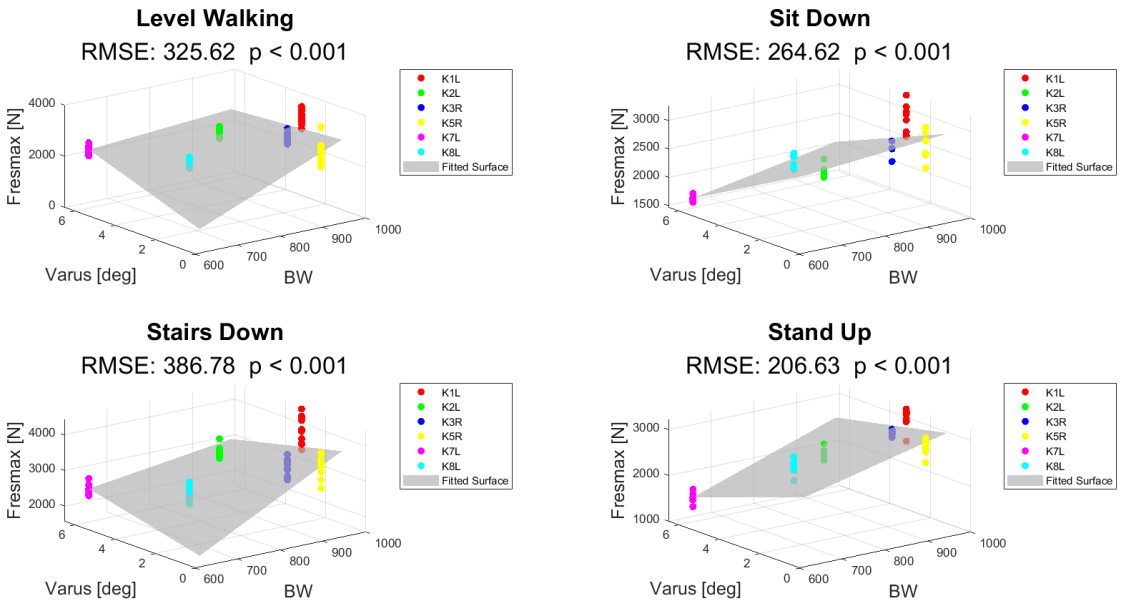

Figure 38: Multiple linear correlation between maximal resultant force in the joint (registered by knee implant), bodyweight and varus angle for all activities from the patient's cohort.

5.3 Limitations and Discussion

Assessing the impact of different physiological variables on joint loading is a relevant topic to better understand the fracture healing process in its entirety. Especially the exact regulation of internal forces is unclear during the rehabilitation period, as we still cannot predict local forces and deformations in fracture patients. However, the healing models based on strain strongly depend on those macroscopic biomechanical parameters.

Despite the use of a simple linear regression model to fit joint loading forces with body weight, varus angle and combination of both, useful insights could be highlighted.

Body weight plays obviously a crucial role on the development of bone callus in the fracture site and patients need to consciously rehabilitate after surgical treatments, since it's the main element influencing the load transmission at that level. However, even if varus knee angle alone didn't significantly impact the resulting load, its contribution can't be ignored (as it's known to be detrimental for fracture healing) if combined with all the other variables present during motor activities (weight primarily). Coefficients of determination proved the same hypothesis, body weight and combined weight-varus better fit the linear model, rather than force-varus angle. Lastly, RMSE values were relatively high, confirming how the linear model was a standard way to compare physiological variables, but still useful to detect how they affected the resulting force at the joint level.

Future studies involving more complex models and additional variables as gait speed or maximum knee flexion angle could provide further information on how the loading transmission can be influenced and so the bone healing process. Also, analysing motor tasks involving walking aids (such as crutches) could help achieving more reliable and inherent results.

6. CONCLUSIONS

The thesis' objective was exploring and understanding more deeply the variables able to influence the bone healing process, with a specific focus on fracture fixation treatments on the femur and tibia.

In the radiologic image study, it was possible to visually detect the healing stages in a sizable and diverse cohort, concerning tibia and femur fractures treated mostly with intramedullary nails and metal plates. The study findings indicated that plate treatments were more frequently excluded from ratings due to challenges in accurately rating bone fractures by experts, with lowest Intraclass Correlation Coefficients (ICCs), particularly in the lateral and posterior cortices, due to the visual obstruction of cortex due to the implant. ICC values for total modified Radiographic Union Scale for Tibia (mRUST) ratings were higher than the specific callus sides, possibly due to aggregation of scores reducing variability between raters. Further analysis revealed how anatomic reduction strongly influenced the scoring system, this was confirmed assessing ICC again after removing a biased tester. The mRUST scoring system's main limitation lied in its susceptibility to bias based on the clinician's interpretation of callus presence or not in these clinical cases, impacting follow-up stage scores. Despite these limitations, ICCs highlighted good reliability across all cases, confirming the validity of the mRUST scoring system in evaluating fracture healing progression.

Radiological assessment on the same cohort, paired with finite element analysis, showed how bone type and fixation system potentially influenced the callus development. Femur cases exhibited relatively denser and larger calluses compared to tibia cases, but a slower overall healing process was detected. Plate treatments produced large and inhomogeneous calluses, whereas nails and combinations of nail and fibular plate provided greater stability, resulting in more uniform interfragmentary movement and smaller but more regular calluses. These insights were confirmed by the simulation models, where strains onto the gap tissue varied accordingly also depending on gap properties. Furthermore, shear strain in general was associated with somewhat reduced callus formation. However, this second study acknowledged limitations such as idealized implants and loads, as well as the lack of available data for precise callus development analysis in certain follow-up stages.

Lastly, to obtain a wider point of view on the topic, assessing how physiological variables affected joint loading provided additional insights. Despite the use of a simple linear regression model, it was shown that body weight significantly influences bone callus development, emphasizing the need for careful post-surgical rehabilitation. While varus knee angle alone didn't notably affect mechanical loads, its interaction with body weight is important during motor activities. Coefficients of determination supported the results' reliability but need to be considered for its transferability and translation into clinics. Although RMSE values were relatively high, the linear model remained useful to detect a relationship between physiological values and joint loads.

Future studies involving more detailed and specific clinical data, specific and sufficiently complex models with additional elements could provide further discoveries onto loading transmission and variables affecting bone fracture healing process.

REFERENCES

[1] V. J. Alentado *et al.*, 'Validation of the modified radiographic union score for tibia fractures (mRUST) in murine femoral fractures', *Frontiers in Endocrinology*, vol. 13, 2022, Accessed: Oct. 17, 2023. [Online]. Available: https://www.frontiersin.org/articles/10.3389/fendo.2022.911058

[2] L. Audigé, C.-P. Cornelius, A. D. Ieva, and J. Prein, 'The First AO Classification System for Fractures of the Craniomaxillofacial Skeleton: Rationale, Methodological Background, Developmental Process, and Objectives', *Craniomaxillofac Trauma Reconstr*, vol. 7, no. Suppl 1, pp. S006-S014, Dec. 2014, doi: 10.1055/s-0034-1389556.

[3] P. Augat *et al.*, 'Biomechanical methods for the assessment of fracture repair', *Injury*, vol. 45, pp. S32–S38, Jun. 2014, doi: 10.1016/j.injury.2014.04.006.

[4] A. Bigham-Sadegh and A. Oryan, 'Basic concepts regarding fracture healing and the current options and future directions in managing bone fractures', *International Wound Journal*, vol. 12, no. 3, pp. 238–247, 2015, doi: 10.1111/iwj.12231.

[5] A. Bigham-Sadegh, A. Oryan, P. Mirshokraei, M. Shadkhast, and E. Basiri, 'Bone tissue engineering with periosteal-free graft and pedicle omentum', *ANZ Journal of Surgery*, vol. 83, no. 4, pp. 255–261, 2013, doi: 10.1111/j.1445-2197.2012.06316.x.

[6] S. T. Campbell, L. H. Goodnough, B. Salazar, J. F. Lucas, J. A. Bishop, and M. J. Gardner, 'How do pilon fractures heal? An analysis of dual plating and bridging callus formation', *Injury*, vol. 51, no. 7, pp. 1655–1661, Jul. 2020, doi: 10.1016/j.injury.2020.04.023.

[7] E. Cekiç, E. Alıcı, and M. Yeşil, 'Reliability of the Radiographic Union Score for Tibial Fractures', *Acta orthopaedica et traumatologica turcica*, vol. 48, pp. 533–40, Nov. 2014, doi: 10.3944/AOTT.2014.14.0026.

[8] T. R. Chikate and L. Tang, 'Tracking and Imaging of Transplanted Stem Cells in Animals', in *Imaging and Tracking Stem Cells: Methods and Protocols*, K. Turksen, Ed., in Methods in Molecular Biology. , New York, NY: Springer US, 2020, pp. 45–56. doi: 10.1007/7651_2019_275.

[9] M. E. Cooke *et al.*, 'Correlation between RUST assessments of fracture healing to structural and biomechanical properties', *Journal of Orthopaedic Research*, vol. 36, no. 3, pp. 945–953, 2018, doi: 10.1002/jor.23710.

[10] Cristofolini Luca, 'Slides of "Mechanics of Biological TIssues"', 2022.

[11] D. Deppe *et al.*, 'Callus size and density after lower-limb fracture fixation is affected by local loading', 2024 (ongoing publication).

[12] M. Dhillon, *First Aid and Emergency Management in Orthopedic Injuries*. 2012.

[13] G. I. Drosos, M. Bishay, I. A. Karnezis, and A. K. Alegakis, 'Factors affecting fracture healing after intramedullary nailing of the tibial diaphysis for closed and grade I open fractures', *The Journal of Bone & Joint Surgery British Volume*, vol. 88-B, no. 2, pp. 227–231, Feb. 2006, doi: 10.1302/0301-620x.88b2.16456.

[14] G. N. Duda, B. Bartmeyer, S. Sporrer, W. R. Taylor, M. Raschke, and N. P. Haas, 'Does partial weight bearing unload a healing bone in external ring fixation?', *Langenbecks Arch Surg*, vol. 388, no. 5, pp. 298–304, Oct. 2003, doi: 10.1007/s00423-003-0386-2.

[15] G. N. Duda, S. Geissler, S. Checa, S. Tsitsilonis, A. Petersen, and K. Schmidt-Bleek, 'The decisive early phase of bone regeneration', *Nat Rev Rheumatol*, vol. 19, no. 2, pp. 78–95, Feb. 2023, doi: 10.1038/s41584-022-00887-0.

[16] T. A. Einhorn and L. C. Gerstenfeld, 'Fracture healing: mechanisms and

interventions', *Nat Rev Rheumatol*, vol. 11, no. 1, Art. no. 1, Jan. 2015, doi: 10.1038/nrrheum.2014.164.
[17] H. M. Frost, 'Bone dynamics in metabolic bone disease', *J Bone Joint Surg Am*, vol. 48, no. 6, pp. 1192–1203, Sep. 1966.
[18] P. V. Giannoudis, T. A. Einhorn, and D. Marsh, 'Fracture healing: The diamond concept', *Injury*, vol. 38, pp. S3–S6, Sep. 2007, doi: 10.1016/S0020-1383(08)70003-2.
[19] B. Heinlein *et al.*, 'ESB clinical biomechanics award 2008: Complete data of total knee replacement loading for level walking and stair climbing measured in vivo with a follow-up of 6–10 months', *Clinical Biomechanics*, vol. 24, no. 4, pp. 315–326, May 2009, doi: 10.1016/j.clinbiomech.2009.01.011.
[20] M. O. Heller *et al.*, 'A new model to predict in vivo human knee kinematics under physiological-like muscle activation', *Journal of Biomechanics*, vol. 40, pp. S45–S53, Jan. 2007, doi: 10.1016/j.jbiomech.2007.03.005.
[21] M. Heyland, 'Brief Commentary on Mechano-Biological Fixation', *Journal of Investigative Surgery*, vol. 32, no. 3, pp. 255–256, Apr. 2019, doi: 10.1080/08941939.2017.1406018.
[22] M. Heyland *et al.*, 'Validation of mRUST score as endpoint for a fracture healing study', 2024 (ongoing publication).
[23] M. Heyland *et al.*, 'Lower-limb internal loading and potential consequences for fracture healing', *Frontiers in Bioengineering and Biotechnology*, vol. 11, 2023, Accessed: Oct. 30, 2023. [Online]. Available: https://www.frontiersin.org/articles/10.3389/fbioe.2023.1284091
[24] M. Heyland *et al.*, 'Semi-rigid screws provide an auxiliary option to plate working length to control interfragmentary movement in locking plate fixation at the distal femur', *Injury*, vol. 46, pp. S24–S32, Oct. 2015, doi: 10.1016/S0020-1383(15)30015-2.
[25] A. Joeris *et al.*, 'The impact of the AO Foundation on fracture care: An evaluation of 60 years AO Foundation', *Injury*, vol. 50, no. 11, pp. 1868–1875, Nov. 2019, doi: 10.1016/j.injury.2019.07.016.
[26] I. Kaczmarczyk-Sedlak, M. Zych, K. Rotko, and L. Sedlak, 'Effects of thalidomide on the development of bone damage caused by prednisolone in rats', *Pharmacol Rep*, vol. 64, no. 2, pp. 386–395, 2012, doi: 10.1016/s1734-1140(12)70779-x.
[27] A. H. Karladani, H. Granhed, J. Kärrholm, and J. Styf, 'The influence of fracture etiology and type on fracture healing: a review of 104 consecutive tibial shaft fractures', *Arch Orth Traum Surg*, vol. 121, no. 6, pp. 325–328, Jun. 2001, doi: 10.1007/s004020000252.
[28] I. Kutzner *et al.*, 'Loading of the knee joint during activities of daily living measured in vivo in five subjects', *J Biomech*, vol. 43, no. 11, pp. 2164–2173, Aug. 2010, doi: 10.1016/j.jbiomech.2010.03.046.
[29] J. Litrenta *et al.*, 'Determination of Radiographic Healing: An Assessment of Consistency Using RUST and Modified RUST in Metadiaphyseal Fractures', *Journal of Orthopaedic Trauma*, vol. 29, no. 11, p. 516, Nov. 2015, doi: 10.1097/BOT.0000000000000390.
[30] T. J. Lujan, C. E. Henderson, S. M. Madey, D. C. Fitzpatrick, J. L. Marsh, and M. Bottlang, 'Locked Plating of Distal Femur Fractures Leads to Inconsistent and Asymmetric Callus Formation', *Journal of Orthopaedic Trauma*, vol. 24, no. 3, p. 156, Mar. 2010, doi: 10.1097/BOT.0b013e3181be6720.
[31] S. Märdian, K.-D. Schaser, G. N. Duda, and M. Heyland, 'Working length of locking plates determines interfragmentary movement in distal femur fractures

under physiological loading', *Clinical Biomechanics*, vol. 30, no. 4, pp. 391–396, May 2015, doi: 10.1016/j.clinbiomech.2015.02.006.
[32] R. Marsell and T. A. Einhorn, 'The biology of fracture healing', *Injury*, vol. 42, no. 6, pp. 551–555, Jun. 2011, doi: 10.1016/j.injury.2011.03.031.
[33] S. Mirhadi, N. Ashwood, and B. Karagkevrekis, 'Factors influencing fracture healing', *Trauma*, vol. 15, no. 2, pp. 140–155, Apr. 2013, doi: 10.1177/1460408613486571.
[34] A. Oryan, S. Alidadi, A. Moshiri, and N. Maffulli, 'Bone regenerative medicine: classic options, novel strategies, and future directions', *Journal of Orthopaedic Surgery and Research*, vol. 9, no. 1, p. 18, Mar. 2014, doi: 10.1186/1749-799X-9-18.
[35] A. Oryan, A. Moshiri, and S. Alidadi, 'Current concerns regarding healing of bone defects', *Hard Tissue*, vol. 2, p. 13, Feb. 2013, doi: 10.13172/2050-2303-2-2-374.
[36] A. M. Parizi, A. Oryan, Z. Shafiei-Sarvestani, and A. S. Bigham, 'Human platelet rich plasma plus Persian Gulf coral effects on experimental bone healing in rabbit model: radiological, histological, macroscopical and biomechanical evaluation', *J Mater Sci: Mater Med*, vol. 23, no. 2, pp. 473–483, Feb. 2012, doi: 10.1007/s10856-011-4478-1.
[37] S. M. Perren, 'Hojení zlomenin: kostní hojení jako výsledek fascinující kaskády fyzikálních a biologických interakcí. Část II', *ACHOT*, vol. 82, no. 1, pp. 13–21, Feb. 2015, doi: 10.55095/achot2015/002.
[38] J. C. Reichert *et al.*, 'A Tissue Engineering Solution for Segmental Defect Regeneration in Load-Bearing Long Bones', *Science Translational Medicine*, vol. 4, no. 141, pp. 141ra93-141ra93, Jul. 2012, doi: 10.1126/scitranslmed.3003720.
[39] A. Remedios, 'Bone and Bone Healing', *Veterinary Clinics of North America: Small Animal Practice*, vol. 29, no. 5, pp. 1029–1044, Sep. 1999, doi: 10.1016/S0195-5616(99)50101-0.
[40] P. Seebeck, M. S. Thompson, A. Parwani, W. R. Taylor, H. Schell, and G. N. Duda, 'Gait evaluation: A tool to monitor bone healing?', *Clinical Biomechanics*, vol. 20, no. 9, pp. 883–891, Nov. 2005, doi: 10.1016/j.clinbiomech.2005.05.010.
[41] J. R. Sheen, A. Mabrouk, and V. V. Garla, 'Fracture Healing Overview', in *StatPearls*, Treasure Island (FL): StatPearls Publishing, 2023. Accessed: Jan. 21, 2024. [Online]. Available: http://www.ncbi.nlm.nih.gov/books/NBK551678/
[42] A. K. Srivastava and J. W. M. Bulte, 'Seeing Stem Cells at Work In Vivo', *Stem Cell Rev and Rep*, vol. 10, no. 1, pp. 127–144, Feb. 2014, doi: 10.1007/s12015-013-9468-x.
[43] J. Street, D. Winter, J. H. Wang, A. Wakai, A. McGuinness, and H. P. Redmond, 'Is human fracture hematoma inherently angiogenic?', *Clin Orthop Relat Res*, no. 378, pp. 224–237, Sep. 2000, doi: 10.1097/00003086-200009000-00033.
[44] A. L. Strong, M. W. Neumeister, and B. Levi, 'Stem cells and tissue engineering: regeneration of the skin and its contents', *Clin Plast Surg*, vol. 44, no. 3, pp. 635–650, Jul. 2017, doi: 10.1016/j.cps.2017.02.020.
[45] W. R. Taylor *et al.*, 'A comprehensive assessment of the musculoskeletal system: The CAMS-Knee data set', *Journal of Biomechanics*, vol. 65, pp. 32–39, Dec. 2017, doi: 10.1016/j.jbiomech.2017.09.022.
[46] A. Trepczynski *et al.*, 'Patellofemoral joint contact forces during activities with high knee flexion', *Journal of Orthopaedic Research*, vol. 30, no. 3, pp. 408–415, 2012, doi: 10.1002/jor.21540.
[47] A. Trepczynski, I. Kutzner, V. Schwachmeyer, M. O. Heller, T. Pfitzner, and G. N. Duda, 'Impact of antagonistic muscle co-contraction on in vivo knee contact

forces', *Journal of NeuroEngineering and Rehabilitation*, vol. 15, no. 1, p. 101, Nov. 2018, doi: 10.1186/s12984-018-0434-3.
[48] D. B. Whelan *et al.*, 'Development of the Radiographic Union Score for Tibial Fractures for the Assessment of Tibial Fracture Healing After Intramedullary Fixation', *Journal of Trauma and Acute Care Surgery*, vol. 68, no. 3, p. 629, Mar. 2010, doi: 10.1097/TA.0b013e3181a7c16d.
[49] E. A. Zimmermann and R. O. Ritchie, 'Bone as a Structural Material', *Advanced Healthcare Materials*, vol. 4, no. 9, pp. 1287–1304, 2015, doi: 10.1002/adhm.201500070.
[50] [Online]. Available: https://www.orthobullets.com/basic-science/9009/fracture-healing
[51] 'AO/OTA Fracture and Dislocation Classification Compendium—2018'. Accessed: Dec. 19, 2023. [Online]. Available: https://www.aofoundation.org/trauma/clinical-library-and-tools/journals-and-publications/classification
[52] 'CAMS-Knee Project'. Accessed: Jan. 21, 2024. [Online]. Available: https://movement.ethz.ch/data-repository/cams-knee-project.html

ACKNOWLEDGEMENTS

We always say that time flies, but if you just stop for a minute and think about it…it's not true.

These past two and a half years have been the longest and the shortest two and a half years of my life and now, looking back at them… it's hard to ignore a nostalgic feeling. Many things, too many things happened, but each experience brought me to be who I am today.

I deeply thank Professor Luca Cristofolini, for following and guiding me through my internship and Erasmus period, with his availability and support. Thanks to Mark Heyland and Adam Trepczynski and all my colleagues at the JWI, who helped and assisted me during my period in Berlin, allowing me to explore and acquire knowledge on a large variety of clinical sectors and permitting me to take part in publications and research.

I want to acknowledge my parents, my grandparents, and my aunt, who always supported me in any situation (despite their slight doubt on my ability to get by on my own in many complex situations…guess they know it by now). My sister, my light, my pride, being her reference point makes me the happiest and proudest brother in the world.

These years wouldn't have been the same without all my friends: the journeys, the laughs, the emotional/psychological supports, the study meetings in Peppe's living room, the video-calls, the sadness in preparing the last exams together and the affection of my friends, who even flew from Italy to visit me in Berlin.

Last but not least, I want to thank me, I want to thank me for believing in me, I want to thank me for never quitting, for always being true to myself and for risking it, always…because:

Life is a risk worth taking.